Dielectric spectroscopy of organic solvents of varying polarity

by

A Dissertation submitted to the School of Graduate Studies in partial fulfillment of the requirements for the degree of

M.Sc.

Department of Physics and Physical Oceanography
Memorial University of Newfoundland

Memorial University of Newfoundland

April 2016

St. John's Newfoundland

Abstract

The dielectric constant and the conductivity for several organic solvents of varying polarity and for colloidal suspensions are measured using dielectric spectroscopy as a function of frequency, over the frequency range 0.1 Hz to 100 kHz. These measurements are carried out for organic solvents of different polarities: cyclohexyl bromide (CHB), castor oil, cis+trans-decahydronaphtalene (decalin) and decane. In addition, dielectric spectroscopy is carried out for polymethylmethacrylate (PMMA) colloidal spheres in the intermediate polar mixture of cyclohexy bromide (C_6 H_{11} Br,(CHB)) and 20% cis+trans-decalin by volume.

The primary result in this thesis is the examination of electrode polarization effects, which were observed at low frequency in CHB and CHB-decalin mixtures. A simple model function for sample impedance coupled with electrode polarization, involving a power law dependance of the polarization capacitance on frequency, provided an excellent fit to the dielectric spectra at low and high frequencies. These measurements provide direction for future measurement on colloidal suspensions in these solvents.

Acknowledgements

I would to thank first my supervisor Prof. Anand Yethiraj for guidance and encouragement in carrying out this project work. I'm extremely grateful for your assistance and suggestions throughout my project. I also thank Prof. Kris Poduska for providing generous access to their impedance analyzer, and her student Jiaqi Cheng who showed me how to use it. I would thank Gordon Whelan in the machine shop for helping with electrodes for the early versions of the dielectric cell. Deep thanks for all my friends in Anand's group: Suhad Sbeih, Swomitra Palit, Somayeh Tadavani, and Payam Bagheri for providing help in any time. To my family, deep thanks for helping me survive from all these years and not letting me give up. Special thanks to my husband for always listening and giving me words of encouragement. Last but not least, I would like to thank the Ministry of Higher Education, Kingdom of Saudi Arabia for scholarship.

Table of Contents

List of Tables

List of Figures

Chapter 1

Introduction

The dielectric spectroscopy of colloidal suspensions has been a subject of interest in the last decade because it provides an information about the electrokinetic properties of a colloidal dispersions [9, 10]. This has been studied extensively in aqueous systems; non-aqueous dispersions have been less studied.

Dipolar interactions can be induced between colloidal particles by exposing them to an electric field which leads to significant changes in the properties of the colloidal suspension [11, 12]. Under the effect of electric field, directed self-assembly has been obtained from the polarization of the colloidal particles [13, 14]. In aqueous colloidal systems, the application of a field results in the formation of a tetragonal crystal phase [15]. In non-aqueous colloidal suspensions, however, there are; in addition, many other crystalline phases [16].

Dispersions of colloidal particles in a moderate polar medium (one example is the cyclohexyl bromide-decalin mixture) have been condensed matter model systems of considerable interest [12, 17, 18]. This mixture is neither a low polar medium like pure decalin or dodecane nor polar like water or ethanol, and it has unusual electrokinetic properties which are not well understood.

The dielectric spectroscopy of colloidal suspensions in which the suspension environment is controlled with salt (aqueous system) have been investigated. Beltramo and Furst (2012) found that in an aqueous system, at varying frequencies and volume fractions, the electrokinetic properties of the system will change because of the effect of the neighbouring particles on the ionic fluxes [19]. In addition, in non-aqueous system, the dipole moment induced on the colloidal particle by an external electric field is affected by the salt concentration of the background [13]. The original interest for studying a non-aqueous colloidal system in this thesis was that unusual electrokinetic properties were expected, based on observations from microscopy experiments [20] in the presence of low-frequency AC electric field. However, the low-frequency electrokinetic response was masked by a strong electrode polarization effect, which then became the focus of this thesis.

In this work, an impedance analyzer has been used to measure the electrokinetic properties of a non-aqueous system as a function of frequency in the range between 0.1 Hz to 100 kHz. In addition, the essential part of this thesis is that we designed an appropriate cell that can be used more then once. Parallel-plate cells, where each inward-facing glass slide was coated with a transparent but electrically conducting layers of Indium Tin Oxide (ITO), with three different cell thicknesses were made. These cells were easy to fill and empty and could thus be used several times. The main issues that have been faced in the impedance measurements are the noisy data at high frequency, between 10kHz to 100kHz, and the electrode polarization at low frequencies. In addition, a stray capacitance has been observed and corrected in our measurements which affected the electrolyte capacitance and hence the electrolyte dielectric constant.

The key properties that have been measured and analyzed by using the dielectric spectroscopy in this thesis are the dielectric permittivity ε and the conductivity σ. These properties are measured as a function of frequency for 4 organic solvents: cyclohexyl bromide (CHB), cis+trans-decahydronaphtalene (decalin), castor oil and decane.

In our CHB-containing solvents, we observed a phenomenon known as electrode polarization. Decreasing the effect of electrode polarization has been examined by decreasing the concentration of ions and/or increasing the electrode spacing. These strategies are explained in detail here. An existing model was successfully employed to describe the physical phenomena of the dielectric spectra at low and high frequencies.

A minor part of this thesis is about colloids in suspension. Whereas this was originally the primary goal, understanding issues surrounding electrode polarization in particle-free solvents became the primary focus. We studied the dielectric properties of PMMA colloids suspended in CHB-decalin, which is an intermediate polar medium. In addition, the characteristic frequency of the double layer relaxation f_{rel} has been calculated and predicted for our non-aqueous system and compared with that for the aqueous system that was studied by Saville (1990) [12].

Chapter 2

Background and Theory

2.1 Introduction

This chapter provides background about electrokinetic phenomena. It also outlines how the shape of the double layer changes over characteristic frequency regimes. In addition, it describes the fundamentals of the dielectric spectroscopy. Finally, the phenomenon of electrode polarization in dielectric measurement is outlined here.

2.2 Electrokinetic phenomena

Electrokinetic processes arise from the interaction between the electric diffuse layer on a charged particle in a solvent and the resulting ion motion in an electric field [11]. To make this phenomenon clearer, assume that I apply an external field to a charged particle in an ionic solution that is placed between two electrodes. A current will flow because of the presence of the ions in the solution. Applying an external field creates relative motion between the suspended particles and the bulk fluid (electrophoresis), as well as between the particles and the diffuse electric charge of mobile ions surrounding the particles (electro-osmosis) [21]. Thus, the particles and

the charges of the diffuse layer move in opposite directions because of the difference in the sign of their charges. As result, an ionic dipole moment will occur. This dipole-dipole interaction between particles can affect the suspension structure and can give rise to a change in the flow behaviour. The dipolar interaction increases with increasing field strength. At high electric field, the suspension can appear more viscous when applying an electric field and it returns to its original state as soon as the field is switched off. This is known as the electroviscous effect [11]. It should be clarified that the measurements performed in this thesis are for electric fields that are too small to change suspension structure. They are in the "linear response" regime.

2.2.1 Electrophoresis

Electrophoresis can be defined as the motion of the system components (particles, ions, and fluid) under the effect of an external field [22]. Because of the effect of the field on the charges, a force on the particles will result. Thus, the particles will move and drag some fluid with them. Indeed, when a dielectric surface is placed in contact with an ionic solution, the surface will be charged and a cloud of opposite charges will be created around the surface. The measurement of electrophoresis is important because it measures the mobility of the particle charge or Zeta potential of partial-liquid interface, from which we can derive the electrical charge.

2.3 The effect of the double layer system on the electrophoretic mobility

2.3.1 A thin electric double layer

The interaction between colloidal particles in suspension are strongly affected by their electrostatic environment. In a system where the ionic concentration is high (κa $\gg$ 1), the electrostatic double layer is thin. Here κ^{-1} is the Debye screening length and a is the particle radius. The double layer characteristic dimension is given by the Debye length:

$$\kappa^{-1} = \left[\frac{k_B T \varepsilon_m \varepsilon_0}{2Ie^2}\right]^{\frac{1}{2}} . \tag{2.1}$$

Here, the ionic strength $I = \sum_{i=1}^{N}(z_i^2 n_i^{\infty})$, k_B is Boltzmann constant, T is the absolute temperature, ε_0 is the dielectric permittivity of the vacuum, ε_m is the (dimensionless) dielectric constant of the solvent, e is the fundamental charge, z_i is the ion valence, and n_i^{∞} is the concentration of each ionic species. The mobility in the limit of thin double-layers is given by the Smoluchowski equation:

$$\mu = \frac{\varepsilon_m \varepsilon_0 \zeta}{\eta} , \tag{2.2}$$

where ζ is the Zeta potential, which is the potential difference between the dispersion medium and the stationary layer of fluid attached to the dispersed particle, and η is the fluid viscosity.

2.3.2 A thick electric double layer

If the double layer is thick, in the limit κa $\to$ 0, there is no electrokinetic effect. The mobility in the limit of thick double-layers (κa $\ll$ 1) is given by the H$\ddot{u}$ckel equation

[21, 22]:

$$\mu = \frac{2\varepsilon_m \varepsilon_0 \zeta}{3\eta}\,. \tag{2.3}$$

Note that the factor (1 or 2/3) is the only difference between the Smoluchowski and H*ü*ckel equations.

2.4 Henry's function

Henry′s function describes the electrophoretic mobility of a spherical particle at low or constant surface potential. Henry included the local electric field around the particles, which H*ü*ckel and Smoluchowski did not take it into account [22, 23]. The electrophoretic mobility obtained by Henry can be written as

$$\mu = \frac{2\varepsilon_m \varepsilon_0 \zeta}{3\eta}.f_1(\kappa a)\,, \tag{2.4}$$

where, $f_1(\kappa a)$ is Henry′s function which depends on the thickness of the double layer κ^{-1}, and a the particle radius. When the double layer is thick ($\kappa a \ll 1$), $f_1(\kappa a) \to 1$, at which H*ü*ckel mobility can be observed. However, in the case of a thin double layer ($\kappa a \gg 1$), $f_1(\kappa a) \to 3/2$ and Smoluchowski mobility can be achieved.

2.5 The formation of the double layer at the electrode surface over characteristic frequency regimes

2.5.1 At high frequency

In any conductive system that consists of dissolved free ions, the ions stay in random spatial distribution when exposed to a high frequency electric field (Figure 2.1, left

panel); the same formation occurs in equilibrium; i.e. for ions when the electric field is absent. At high frequencies, the ions are not mobile because they do not have sufficient time to respond to the applied field. Furthermore, a polarizability arises from the the difference of the dielectric constant between the particles and the medium. In this case, the suspension behaviour is "electrokinetically dilute" [19]. As a result, the dielectric constant or the capacitance of the sample can be obtained from the high frequency electrokinetic response which is frequency independent above a threshold frequency, as we can see in Figure 2.2 [5].

2.5.2 At low frequency

At low frequencies, the ions have the ability to move and arrange as a layer along the electrode surfaces. As a result, the applied voltage will drop across these layers leading to electrode polarization (Figure 2.1, right panel) [5, 24, 25]. As the frequency decreases, the magnitude of the ionic polarization increases and dominates the signal see Figure 2.2.

Electrode polarization can be corrected by using a number of approaches such as increasing the electrode spacing or decreasing the ionic concentration in the medium. Both approaches were studied in this work.

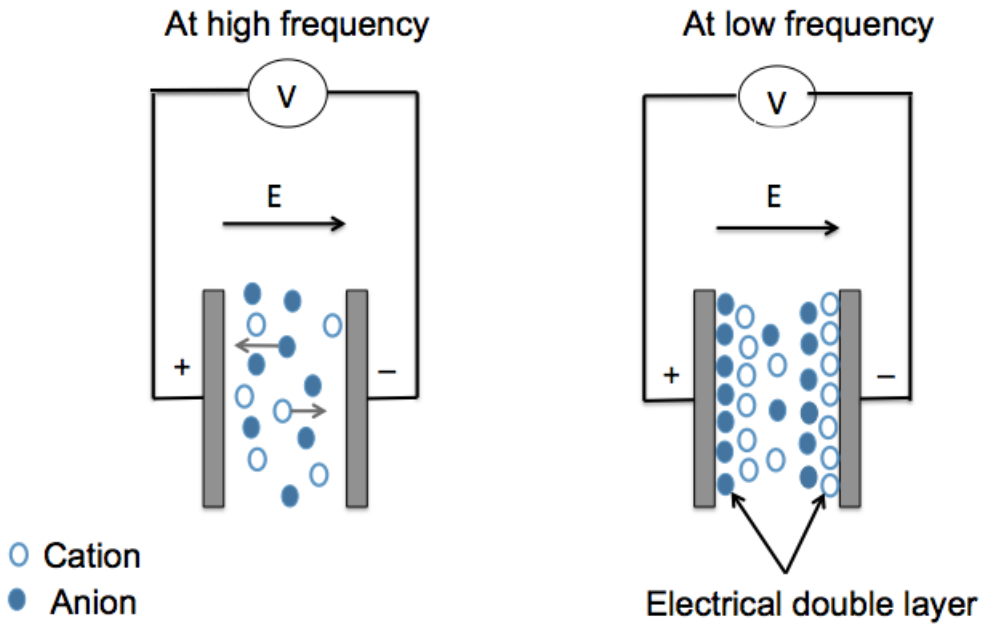

Figure 2.1: Schematic of the formation of the double layer over characteristic frequency regimes. At high frequency, the ions do not have time to move and stay in a random spatial distribution. At low frequency, the ions have time to move and accumulate in the electrodes. Adapted from [5].

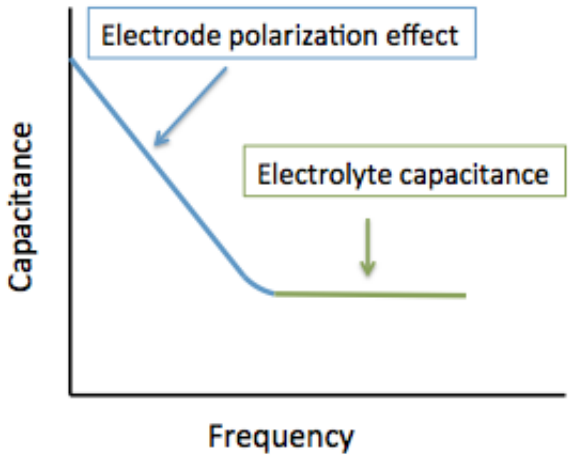

Figure 2.2: Schematic representation of the measured sample capacitance. The effect of electrode polarization is seen at low frequency and the absence of this effect is observed at high frequency where the electrolyte capacitance can be measured. Adapted from [5].

2.6 Impedance Spectroscopy

2.6.1 Background and basic definitions

Impedance spectroscopy is a technique that measures the electrical impedance Z or admittance Y as a function of frequency and analyzes it in a complex impedance plane [26]. The technique is a useful method to characterize many materials' electrical properties and their interfaces with conducting electrodes. Furthermore, impedance spectroscopy is used to study the dynamics of the charge mobility in the bulk for solid or liquid materials, such as, ionic, semiconducting, and dielectric materials. [6]

2.6.2 Responses to a small-signal stimulus in the frequency domain

A common approach to measuring the impedance is by applying a single frequency voltage to the sample. From the resulting current, we can measure the phase shift θ and the amplitude |Z|, or equivalently, the real and imaginary components of the impedance. [6]

When a sinusoidal electrical stimulus is applied (voltage or current) to a cell, in the case of an applied voltage, the signal can be defined by

$$V(t) = V_o \sin(\omega t)\,, \tag{2.5}$$

where $\omega = 2\pi f$ is the angular frequency. Then the responding current is

$$I(t) = I_o \sin(\omega t + \theta)\,, \tag{2.6}$$

where θ is the phase difference between the voltage and the current. After collecting

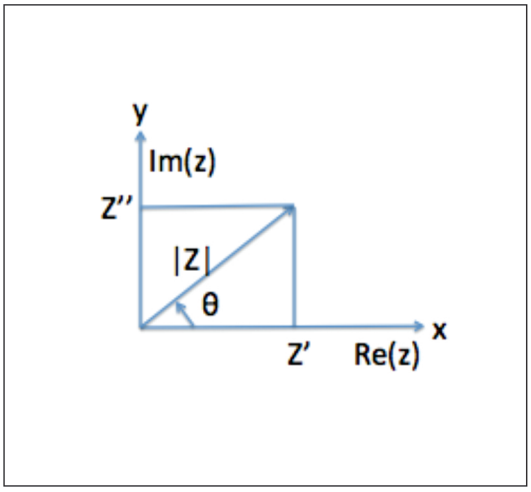

Figure 2.3: Plotting of the impedance Z as a planar vector. Adapted from [6].

the data, the voltage and current are transformed to the frequency domain by applying a Fourier transform. In the frequency domain, the voltage/current relation is formed in similar way to Ohm's law for dc current. The complex impedance Z can be obtained by taking the ratio of the voltage to the current as a complex number

$$Z(\omega) = \frac{V(\omega)}{I(\omega)}\,. \tag{2.7}$$

In ac current, the resistance R is substituted by the impedance Z because it takes phase difference into account. The impedance $Z(\omega)$ is a vector quantity that is plotted in a complex plane with rectangular or polar coordinates, as is shown in Figure 2.3. The complex impedance $Z(\omega)$ can be defined as the sum of the real part Z' and the imaginary part Z'' which are related to the resistance and the capacitance respectively,

$$Z = Z' + jZ''\,, \tag{2.8}$$

where j $= \sqrt{-1}$. The admittance can be defined as $Y = Z^{-1}$. The two rectangular

coordinates can be written as

$$Re(Z) = Z' = |Z|\cos(\theta) \tag{2.9}$$

and

$$Im(Z) = Z'' = |Z|\sin(\theta) \tag{2.10}$$

where the phase angle $\theta = tan^{-1}\ \frac{Z"}{Z'}$ and the amplitude is

$$|Z| = [(Z')^2 + (Z'')^2]^{\frac{1}{2}} \tag{2.11}$$

In polar form, Z can be defined as

$$Z(\omega) = |Z|\exp(j\theta)\,, \tag{2.12}$$

which can be converted to rectangular form by using the Euler relation

$$\exp(j\theta) = \cos(\theta) + j\sin(\theta)\,. \tag{2.13}$$

2.6.3 Dielectric spectroscopy measurements and related functions

Understanding the frequency dependent dielectric constants and effective conductivity functions of solutions confined between electrodes are the main objects of my project. These components can be obtained from the impedance Z. The cell that I use, consisting of a liquid sandwiched between two parallel plate electrodes, has the

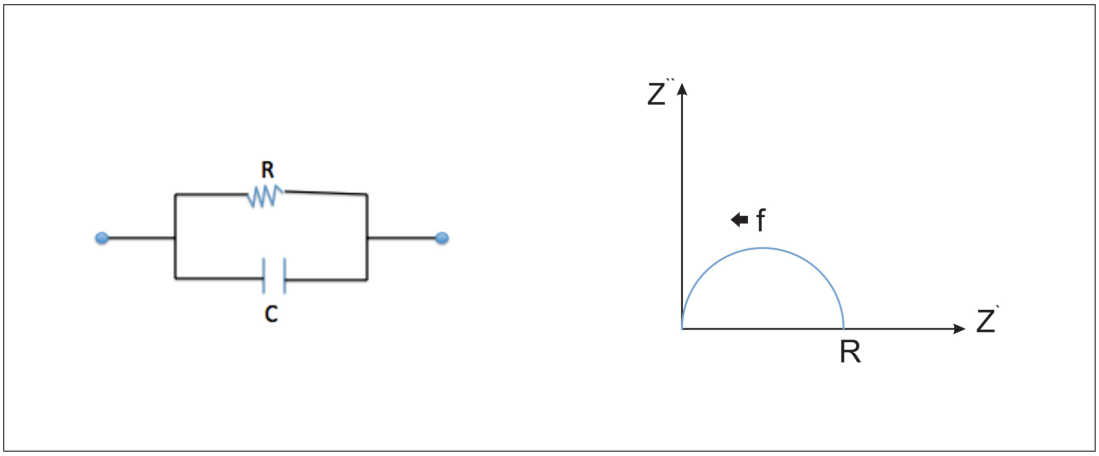

Figure 2.4: Parallel RC circuit and their complex impedance plane plot. Adapted from [6].

equivalent circuit that is shown in the schematic in Figure 2.4. This is a resistor and capacitor in parallel; thus the impedance in equation 2.8 can be written as

$$\frac{1}{Z} = \frac{1}{Z'} + \frac{1}{Z''}\,, \tag{2.14}$$

where the real part of Z represents the resistance and the imaginary part of Z represents the capacitance($Z' = R$ and $Z'' = \frac{-j}{\omega C}$). Here j=$\sqrt{-1}$ and $\omega = 2\pi f$, and we can write

$$\begin{aligned} \frac{1}{Z} &= \frac{1}{R} + j\omega C \\ \frac{1}{Z^*} &= \frac{1}{R} - j\omega C \end{aligned} \tag{2.15}$$

Thus we can write

$$\frac{1}{|Z|^2} = \frac{1}{Z^* Z} = \frac{1}{R^2} + \omega^2 C^2\,, \tag{2.16}$$

and

$$|Z| = \frac{R}{\sqrt{1 + (2\pi R f C)^2}}\,. \tag{2.17}$$

Equation 2.17 is the function that I used to fit the impedance |Z| data as function of frequency. The measurement of the impedance is related to the permittivity and conductivity. Thus, we can measure the conductivity and the dielectric permittivity from the fit parameters the resistance and the capacitance, respectively in the fit function Equation 2.17. While the impedance measurements give us resistance and capacitance (Equation 2.15), we need to relate this to cell geometry independent properties, i.e the conductivity and dielectric constant. We can obtain conductivity from R using the relations

$$R = \left(\frac{1}{\sigma}\right)\left(\frac{d}{A}\right), \tag{2.18}$$

where d is the gap distance between the two parallel plates, A is the cell area, and σ is the conductivity. Similarly, we can obtain the dielectric constant from the capacitance C using the relation

$$C = \varepsilon\varepsilon_o\left(\frac{A}{d}\right), \tag{2.19}$$

where ε is the dielectric constant or the permittivity of the solvent and ε_o is the permittivity of free space. The AC impedance is frequency dependent. By defining R and C from equations 2.18 and 2.19 in equation 2.15, the equation for the (complex) admittance $Y(\omega) = 1/Z(\omega)$ is

$$Y(\omega) \;=\; \frac{1}{Z(\omega)} = G[\sigma(\omega) + j\omega\varepsilon_o\varepsilon_m(\omega)]. \tag{2.20}$$

In the above, G = A/d is known as the cell constant, and has unit of length. The dielectric constant and the conductivity as a function of the frequency can be determined from the imaginary Z'' and real Z' impedance respectively from the equations

$$\varepsilon_m(\omega) = \left(\frac{1}{Z}\right)''\left(\frac{1}{\omega\varepsilon_o G}\right) \tag{2.21}$$

and

$$\sigma(\omega) = \left(\frac{1}{Z}\right)' \left(\frac{1}{G}\right) . \tag{2.22}$$

2.7 The complex dielectric constant and conductivity of any system

The presence of the free ions in solution will influence the current flow through solution in many ways. In general, the response of the system components to the electric field occur in one of two ways. First, there is pure ohmic conduction (at high frequencies), where the charges are free to move; and second there is non-ohmic conduction (polarization effect at low frequencies), where the charges' motion is blocked [7, 27]. These two terms appear in a macroscopic view when the sample is placed in an external electric field.

The complex dielectric function ε^* is frequency dependant and it has components that are in and out of phase with the applied field, which are here written in the "prime" notation as ε' and ε'', the real and imaginary part, respectively,

$$\varepsilon^*(\omega) = \varepsilon'(\omega) - j\varepsilon''(\omega) \tag{2.23}$$

where $(j = \sqrt{-1})$ and $\omega = 2\pi f$. [7]

It has been shown [7] that as the frequency decreases, the imaginary part, ε'', of the complex dielectric function $\varepsilon^*(\omega)$ increases, this is labeled as (1) in the graphs of Figure 2.5. However, in pure ohmic conduction behaviour at high frequencies, the real part is frequency independent, this is labeled as (2) in the graphs of Figure 2.5. In contrast, for non-ohmic conduction at low frequencies (labeled as (1) in Figure 2.6), the real part of $\varepsilon^*(\omega)$ increases as the frequency decreases, this phenomena is

known as electrode polarization [7]. At even higher frequencies, there can be dielectric relaxation processes, which is seen as a stepwise change in ε' and peak in ε''. The complex conductivity can be defined from the following relation

$$\sigma^*(\omega) = \sigma'(\omega) + j\sigma''(\omega) \tag{2.24}$$

Relating Equations 2.23 and 2.24 to the measured impedance (Equation 2.20) we can write

$$\frac{1}{Z(\omega)} = G\sigma^*(\omega) \qquad \text{and} \qquad \frac{1}{Z(\omega)} = jG\omega\varepsilon_o\varepsilon^*(\omega).$$

From this, we can identify $\sigma'(\omega) = \sigma(\omega)$ and $\sigma''(\omega) = \omega\varepsilon_o\varepsilon_m(\omega)$ and $\varepsilon'(\omega) = \varepsilon_m(\omega)$ and $\varepsilon''(\omega) = \frac{1}{\omega\varepsilon_o}(\omega)$. Thus, $\sigma'(\omega)$ can be associated with the real conductivity $\sigma(\omega)$ is related to $\varepsilon''(\omega)$ by the relation

$$\sigma'(\omega) = \omega\varepsilon_o\varepsilon''(\omega) \tag{2.25}$$

When $\varepsilon'' \propto \omega^{-1}$, then σ is constant. When ε'' is constant, then $\sigma \propto \omega$.

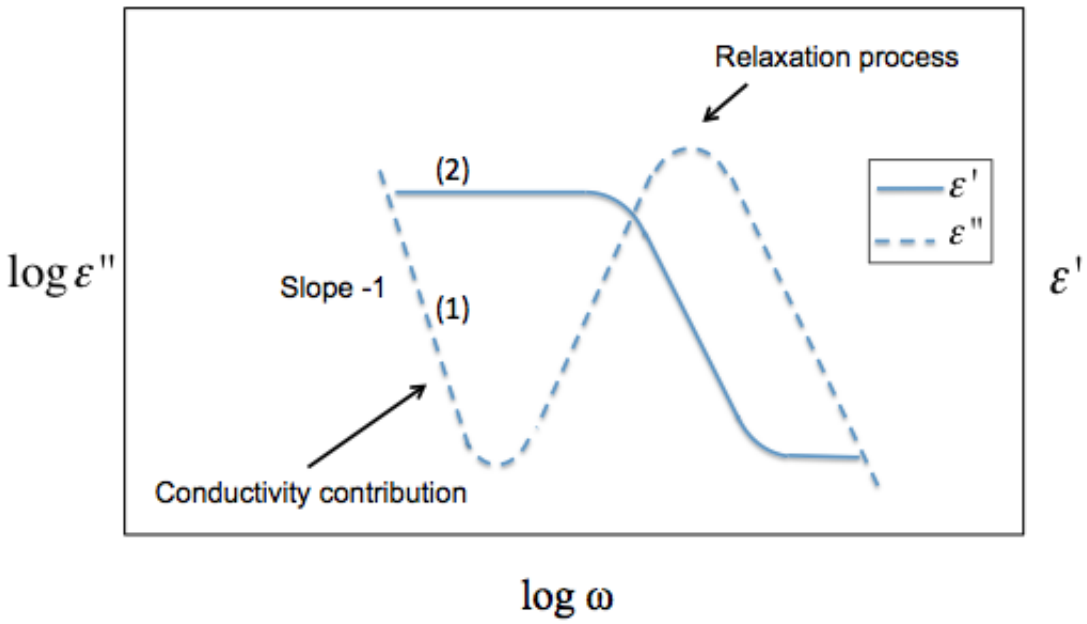

Figure 2.5: Scheme of the relaxation process and the ohmic conductivity of the real ε' (solid line) and imaginary part ε'' (dashed line). Adapted from [7].

2.8 The dielectric relaxation process

Dielectric spectroscopy is mostly used to get information about the dielectric relaxation process due to the fluctuation of molecular dipoles. In the absence of a field, the molecular dipoles are randomly oriented, but in the presence of an external electric field, they will have the direction of the applied electric field. The orientation of the molecular dipole in an electric field requires time which is called the relaxation time τ. By analyzing the complex dielectric function, information about the behaviour of the molecular ensemble can be obtained. The real part of complex dielectric constant $\varepsilon'(\omega)$ decreases step-like as the frequency increases while the imaginary part $\varepsilon''(\omega)$ reaches a maximum (Figure 2.7). The relaxation process can be specified from the dielectric strength $\triangle\varepsilon(\omega)$ that is calculated from the loss peak $\varepsilon''(\omega)$ area or from the step in real part $\varepsilon'(\omega)$.

The typical timescale for relaxation of molecular dipole will be very small. How-

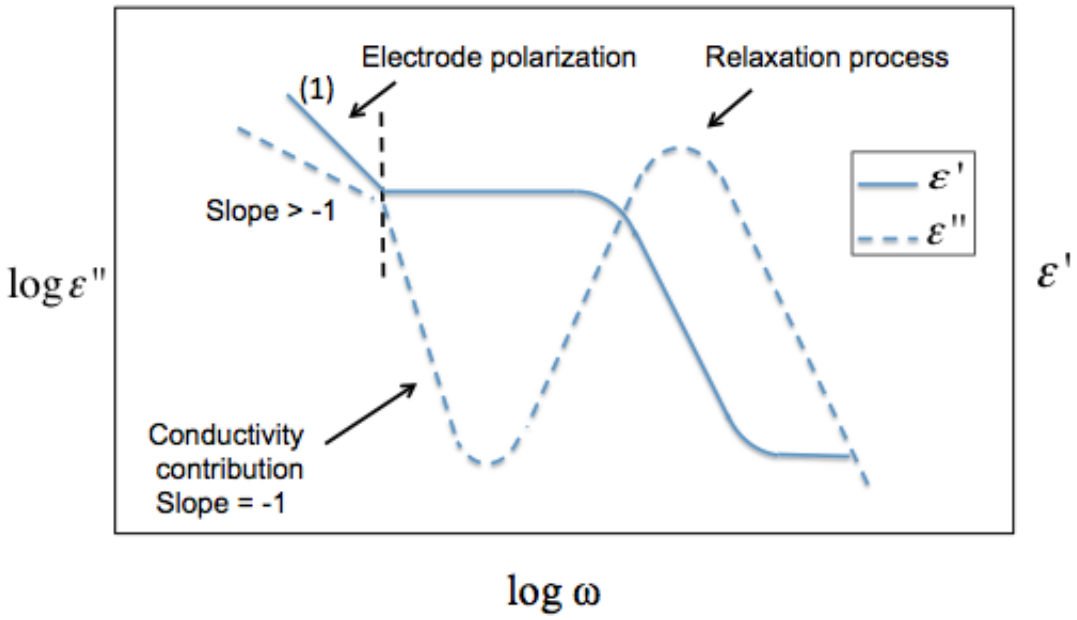

Figure 2.6: Scheme of the relaxation process which behaves as a peak in ε'' and the non-ohmic conductivity of the real ε' (solid line) and imaginary part ε'' (dashed line) of the complex dielectric where the polarization is observed. Adapted from [7].

ever, we can also have dipole induced due to migration of charged species in solution. The characteristic relaxation frequency f_{rel} for this response is typically in the kHz range for an aqueous system [12].

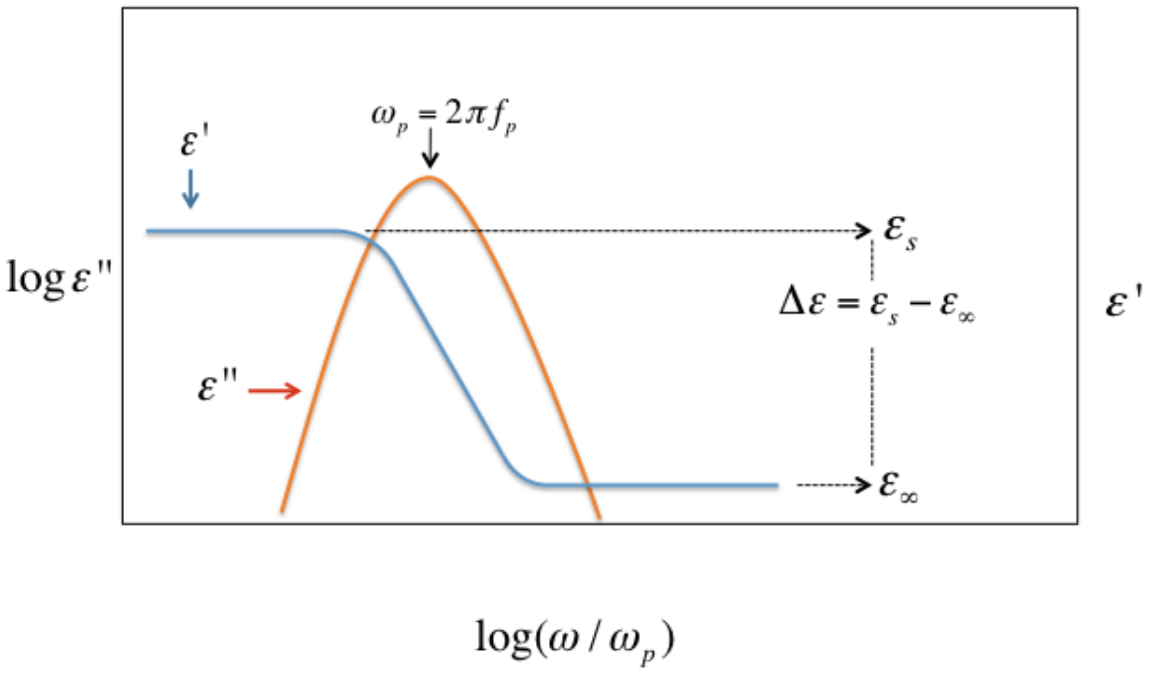

Figure 2.7: The dielectric relaxation process in the real ε' and imaginary part ε'' as a function of frequency. f_p is the frequency of maximal loss, and is associated with the characteristic relaxation frequency, and ε_s is sample's dielectric constant. Adapted from [7].

2.9 Electrode polarization

2.9.1 Electrode polarization definition

Electrode polarization (EP) is a result of accumulation of ions on the electrode's surface. When an electrolyte is placed between electrodes, a potential will be generated due to the distribution of different charges across the interface. Under this electric potential and at low frequency, ions tend to migrate to the electrode/electrolyte interface. As a result, the arrangement of ionic double layers are formed along the electrodes. Along these layers, the potential drop is an exponential decreasing function leading to electrode polarization and absence of the current in the bulk sample. [5, 28, 29]

EP causes errors in determination of impedances of conductive samples, especially in an aqueous and colloidal system [30, 31]. Several experimental techniques methods have been used to correct this effect.

Helmholtz was the first to describe the electrode polarization phenomena [32]. He assumed that there are two layers that are formed along the electrode surface. The first layer is described as the inner layer (Stern layer) of absorbed immobile ions that result from the migration to the surface of electrode under the effect of applied field due to electrostatic forces. Beyond this inner layer is the so-called outer layer (diffuse layer) where the ions in this layer are mobile under the effect of electrostatic forces and diffusion [5, 32]. Then in 1873, a mathematical theory was given by Warburg [33] about the polarization capacitance. Warburg showed that an electrode-electrolyte interface that is impenetrable by ions may be modeled as resistance R and a fequency-depnedent capacitance C in series. The Warburg model is valid at low current density, with both the reactance $X_c = \frac{1}{2\pi f C}$ and resistance R varying inversely with $\sqrt{f}$. However, Fricke [34] and Schwan [35] concluded that R and X_c do not vary with $\sqrt{f}$

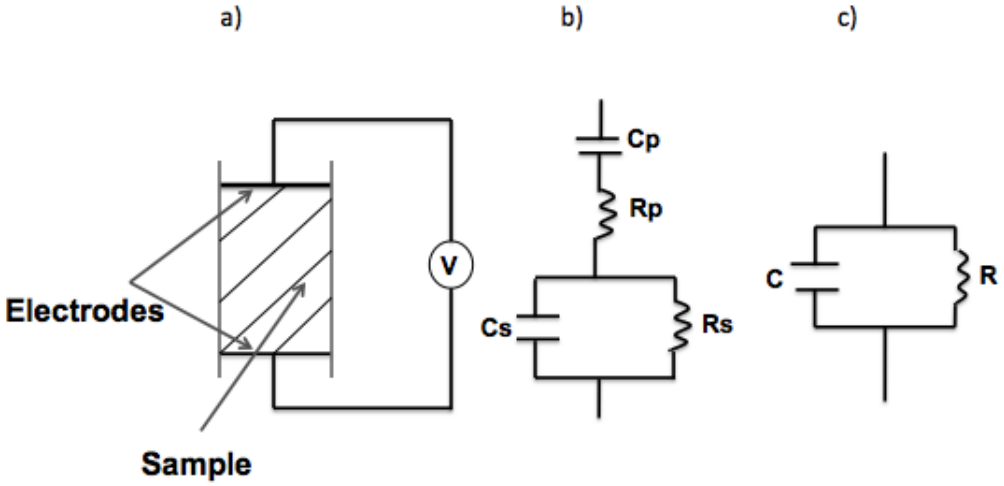

Figure 2.8: a) Sample in contact with electrode. b) Equivalent circuit. The series impedance polarization components R_p and C_p are drawn in series with the parallel sample resistance R_s and capacitance C_s. c) The total admittance of a parallel RC circuit. Adapted from [8].

but instead as $R = A/f^{\alpha}$ and $X_c = B/f^{\beta}$.

2.9.2 Equivalent RC circuit models

A pure dielectric liquid would simply give rise to a capacitance, while one with a small conductivity (large resistivity) would also have a dc resistance. In Figure 2.8, this is represented by the parallel sample resistance R_s and capacitance C_s. On the other hand, polarization charge collects close to the electrode in a thin layer therefore the dc resistance is small. Any resistance would come from the the contact, in series with the polarization capacitance. Thus, the impedance polarization components R_p and C_p are drawn in series. By taking the sum of the polarization admittance and sample admittance we can get the total admittance by the following process. From figure 2.8 (c), the total admittance of an equivalent parallel RC circuit is written as

$$Y = \frac{1}{Z} = \frac{1}{R} + j\omega C \tag{2.26}$$

$$Z = \frac{1}{\frac{1}{R} + j\omega C} \tag{2.27}$$

$$Z = \frac{\frac{1}{R} - j\omega C}{\frac{1}{R^2} + (\omega C)^2} \tag{2.28}$$

$$Z = \frac{R - j\omega R^2 C}{1 + (\omega RC)^2} \tag{2.29}$$

$$Z = \frac{R}{1 + (\omega RC)^2} - \frac{j\omega R^2 C}{1 + (\omega RC)^2} \tag{2.30}$$

We take the sum of the polarization admittance and sample admittance as seen in Figure 2.8 (b), where the parallel sample admittance is written as

$$Y_s = \frac{1}{R_s} + j\omega C_s \tag{2.31}$$

and the series polarization admittance Y_p is given by

$$\frac{1}{Y_p} = R_p + \frac{1}{j\omega C_p}\,. \tag{2.32}$$

Then the summation of Equation 2.32 and 2.31 gives

$$Z = \frac{1}{Y_p} + \frac{1}{Y_s} \tag{2.33}$$

which gives

$$Z = \left(R_p + \frac{1}{j\omega C_p}\right) + \left(\frac{1}{\frac{1}{R_s} + j\omega C_s}\right)\,, \tag{2.34}$$

which can also be written as

$$Z = \left(R_p - \frac{j}{\omega C_p}\right) + \left(\frac{\frac{1}{R_s} - j\omega C_s}{(\frac{1}{R_s})^2 + (\omega C_s)^2}\right)\,. \tag{2.35}$$

Collecting real and imaginary parts, we get

$$Z = \left(R_p + \frac{\frac{1}{R_s}}{(\frac{1}{R_s})^2 + (\omega C_s)^2} \right) - j \left(\frac{\omega C_s}{(\frac{1}{R_s})^2 + (\omega C)^2} + \frac{1}{\omega C_p} \right) \tag{2.36}$$

By taking the first term in Equation 2.36 to equal the first term in Equation 2.30, we get

$$\frac{R}{1 + (\omega RC)^2} = R_p + \frac{R_s}{1 + (\omega R_s C_s)^2} \tag{2.37}$$

$$R = \left[1 + (\omega RC)^2 \right] \left[R_p + \frac{R_s}{1 + (\omega R_s C_s)^2} \right] . \tag{2.38}$$

Similarly, taking the second term in Equation 2.36 to be equal to the second term in Equation 2.30, we get

$$\frac{\omega R^2 C}{1 + (\omega RC)^2} = \frac{\omega C_s R_s^2}{1 + (\omega R_s C_s)^2} + \frac{1}{\omega C_p} . \tag{2.39}$$

Equation 2.39 can be written as

$$\frac{1}{\omega C} = \left[\frac{1}{(\omega RC)^2} + 1 \right] \left[\frac{1}{\omega C_p} + \frac{\omega C_s R_s^2}{1 + (\omega R_s C_s)^2} \right] . \tag{2.40}$$

Equations 2.38 and 2.40 are the measured resistance and capacitance respectively including the effect of the electrode polarization.[36]

In order to describe the impedance behaviour, we derived the following model function that was taken from Equations 2.38 and 2.40. By dividing Equations 2.40 on Equations 2.38 and 2.40, we will get the measured ωRC

$$R\omega C = \frac{\left(\frac{1}{\omega C_p} + \frac{1/\omega C_s}{1+(1/R_s \omega C_s)^2} \right)}{\left(R_p + \frac{R_s}{1+(R_s \omega C_s)^2} \right)} \tag{2.41}$$

This is the fit function that is used in our analyzing for the measuring ωRC as a func-

tion of frequency. Note that R and C the left hand side are the measured quantities, while the quantities on the right hand side are the quantities we need to know.

For most samples which are highly conductive, the electrode polarization effect is higher than that in low conductivity samples [8]. In fact, the electrode polarization is influenced by two factors, which are the concentration of ions in the sample and the electrode separation [8, 24, 35, 36, 37]. In general, the resultant capacitance and resistance increases as the frequency decreases. A study by Schwan (1968) found that the contribution of C_p, to C, that is observed due to the effect of the polarization at low frequencies is larger than the contribution R_p that is observed, to R, in most aqueous systems [24].

2.10 Colloids in CHB-decalin mixtures

Several experiments have been carried for colloids in CHB-decalin mixtures [11, 17, 22]. The solvent is neither a low polarity solvent like pure decalin or dodecane nor polar like water or ethanol, but has intermediate polarity. The colloids in these intermediate polarity solvents have unusual electrokinetic properties which are not well understood. Most dielectric spectroscopy measurement in the past have been carried out an aqueous suspensions. Probing electrokinetics in these intermediate-polarity solvents represents an interesting challenge.

Chapter 3

Experimental Method

3.1 Introduction

The dielectric spectroscopy experiments were carried out by exposing several organic solvents to a frequency dependent electric field. This chapter provides a details of the cell design and construction. Also this chapter presents a brief description of the experimental technique and samples preparation. In addition, issues with noise at particular frequencies are also discussed here.

3.2 Design of the Dielectric Cells

3.2.1 Indium Tin Oxide (ITO)

A glass plate with one side coated with indium tin oxide (ITO), which is a conducting surface with resistance of 20 to 30 Ω, was used in our experiments. An area of $(0.95\times10^{-4}m^2)$ of the coated area was removed using HCl solvent, in order to prevent the current to flow in the uncoated area, as seen in Figure 3.1 (b), leaving a small areas to place the wires. I designed three different cells, each with different gap thickness,

but the same area. The cell thickness was measured by focussing on the top and bottom plates with the sample mounted on an the optical microscope (Nikon Eclipse 80-i upright microscope). Table 3.1 has the values of A and d of the three cells. The cells were made from several layers of microscopic or cover slides and ITO glass in between as shown in figure 3.1 (a). The first layer consist of two microscopic slides, as upper and bottom plates, each 1mm in thickness. The second layer is two slides of ITO glass that were glued (from the sides that are uncoated) to these microscopic slides using UV 86 glue. The coated areas are faced to each other with free space in between. The cell thickness was constructed by building up 3 microscopic slides of 1mm in thickness and area of ($3.5 \times 10^{-4} m^2$) on the two edges of the microscopic bottom plate. This is the thickness of cell number 21 and it is about 614 μm. For the cell number 20 and 22, I decreased the cell thickness by adding additional cover slides of 100 and 170 μm (#0 and #1 cover slide, respectively) between the ITO glass and the upper microscopic slides. All three cells can be used more than once because the cell was designed such that the top plate and the bottom plate can be separated, allowing for the contact area to be cleaned with ethanol between uses. The cell was held together by small clips as shown in Figure 3.2 to ensure that when the electrolytes were added, the cell thickness did not change. Hookup wires were soldered on the ITO plates. The following equation can be used to estimate the cell thickness:

$$\begin{aligned} \text{Cell thickness (d)} = {} & \text{3mm (3 microscopic slides, 1mm for each)} \\ & - \text{2.2mm (2 ITO glass, 1.1mm for each)} \\ & - X \end{aligned} \tag{3.1}$$

where X is the the thickness of additional microscopic cover slides (#0 and/or #1). So as I add more slides, I will decrease the cell thickness. As mentioned, the actual thickness was determined after assembly.

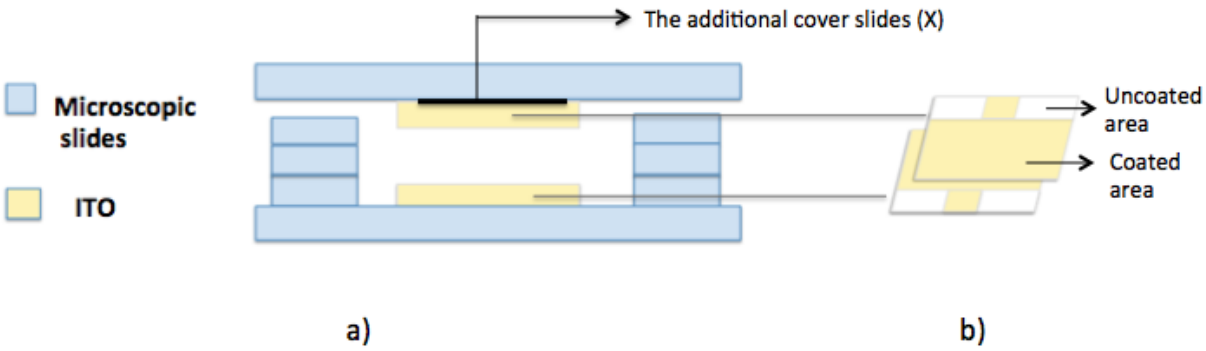

Figure 3.1: (a) Schematic representation of the side view of the cell. X denotes the thickness of the additional cover slides used to control the total gap spacing. (b) The upper and bottom plates of ITO, where the yellow colour represents the conducting area while the white colour represents the nonconducting area.

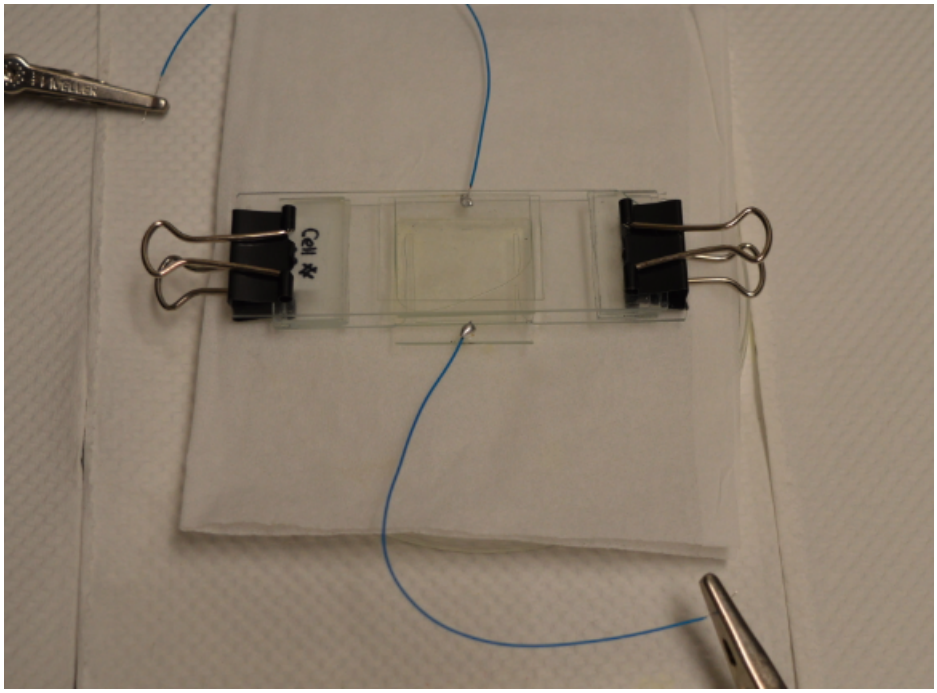

Figure 3.2: A direct view of the cell. The cell is connected to the impedance analyzer and held by small clips.

Table 3.1: The measurement of d and A for three cells. The cell thickness d was measured using Z-focus control of the optical microscope

cell#	d (μm)	A (m^2)	G = A/d (m)
cell#20	355±5	5×10^{-4}	1.42±0.01
cell#21	614±4	5×10^{-4}	0.801 ± 0.005
cell#22	287±2	5×10^{-4}	1.73 ±0.01

3.3 Sample preparation:

Dielectric spectroscopy measurements were made of several organic solvents of varying polarity: cyclohexyl bromide (CHB), cis+trans-decahydronaphtalene (decalin), decane, all from Sigma-Aldrich, and castor oil (Now brand), as well as mixtures of CHB-decalin and dodecane-CHB of several volume fractions. All solvents were used as received. The two mixtures of decalin-CHB and dodecane-CHB were prepared as a series with increasing weight fraction of decalin and dodecane respectively. The mixtures were immediately used for dielectric spectroscopy after preparation.

In the last part of this thesis, we studied the dielectric response of colloidal suspensions. Polymethylmethacrylate (PMMA 447) spheres particles, see Table 3.4, were used in this study. We suspended the particles in intermediate polar medium, which is a mixture of 80 % cyclohexyl bromide (C_6H_{11}Br, (CHB)) and 20% cis+trans-decahydronaphtalene (decalin) by volume. As received, the particles are stored in decalin solvent. Thus, the particles were dried from decalin by exposing them to room temperature and under a nitrogen flush. The dried particles were suspended in (80% CHB-20% decalin) solvent and mixed for one to two minutes by using a vortex mixer. We avoided dispersing the particles by sonicating them to prevent decomposition of the solvent. It has been found that sonication results in an increase in the conductivity of the CHB solvent [Andy Hollingsworth, private communication]. The suspension was immediately loaded into the dielectric spectroscopy cell after the

mixing process.

3.4 Dielectric Spectroscopy

The impedance spectroscopy set up shown in Figure 3.3 was tested and calibrated by measuring known solvents such as pure castor oil, pure CHB, decalin, and decane. The raw data (impedance magnitude |Z|, the real Z', and imaginary parts of the impedance Z'', θ, the real part of the capacitance C', and the imaginary part of the capacitance C'') are collected by using the PowerSUITE software at frequencies ranging between 100 mHz and 100 kHz. A single sine wave was applied for all the measurements at voltage of 1V. Each single measurement was repeated 4 times using the "quality data" selection which is a particular signal averaging option in the PowerSUITE software each experiment takes 20 minutes to collect 30 points between 0.1 Hz to 100 kHz. The cells were disconnected after every measurement to clean the cell surface and check the connection electrode.

Figure 3.3: A potentiostat/galvanostat (Princeton Applied Research model 273A) attached to a lock-in amplifier (Signal Recovery model 5210) was used as an impedance spectrometer.

3.4.1 Instrument calibration and modifications

It was found that the spectrum gave very noisy data both at very low and very high frequencies. This affected our experimental method, and is discussed here. A "dummy cell" was made in order to check if the noisy data comes from the impedance spectrum or from the electrolytes. The dummy cell was simply a resistor and capacitor in parallel. The resistance of the dummy cell was 100 MΩ and the capacitance was 10 pF. From the capacitance measurement, Figure 3.4 (a), we found that the instrument is noise between 0.1 Hz and 3 Hz. In Figure 3.4 (b), the resistance plot displays

noise at high frequencies in the frequency range between 10^3 and 10^5 Hz. Indeed, an experiment on castor oil done on a different dielectric spectrometer (A. Yethiraj, unpublished, Novocontrol Alpha-a, Surajit Dhara lab, University of Hyderabad) was compared with my measurements as seen in Figure 3.5. In Figure 3.5, comparison of resistances shows that our impedance analyzer is significantly noisier between 10^3 and 10^5 Hz. This issue will have to be addressed in future work.

The electrolyte capacitance that was measured by the impedance spectrum was corrected because we realized that the spectra gave higher values than the absolute values predicted. We assumed there is a stray capacitance C^{stray} that was affecting our measurements which comes from contact impedances and/or from fringe-field capacitances through the air or glass. The value of the stray capacitance was defined using two methods. In the first method, we calculated the capacitance C_{calc} of the known cell thickness and area as shown in Table 3.1 of the empty cell. Then we calculated the stray capacitance of $\sim$ 9.3 pF (for cell#22) by subtracting the calculated value capacitance from the spectra measurement capacitance of the same empty cell ($C^{stray} = C_{meas} - C_{calc}$). In the second method, we measured the stray capacitance of $\sim$ 8 pF by measuring the "open circuit" in the contacts to the sample detached. Table 3.1 shows the dielectric constant, $\epsilon_{plateau}$, for different solvents. This is obtained by subtracting C^{stray} from the high-frequency plateau value of the measured capacitance. Table 3.2 shows an example of a comparison of the corrections to the dielectric constant of different solvents using the two methods that discussed above. The first method to extract the stray capacitance was used in all our measurements. This comparison shows that the dielectric constants obtained are generally consistent to about 0.1 for most solvents, but only to about 0.4 for CHB. The stray capacitance was subtracted from all of the measured real capacitance data that we collected from

the spectra. The conductivity of our measurement was not affected perhaps because the insulator contributes to capacitance but not to the conductance; and contact resistances are very low.

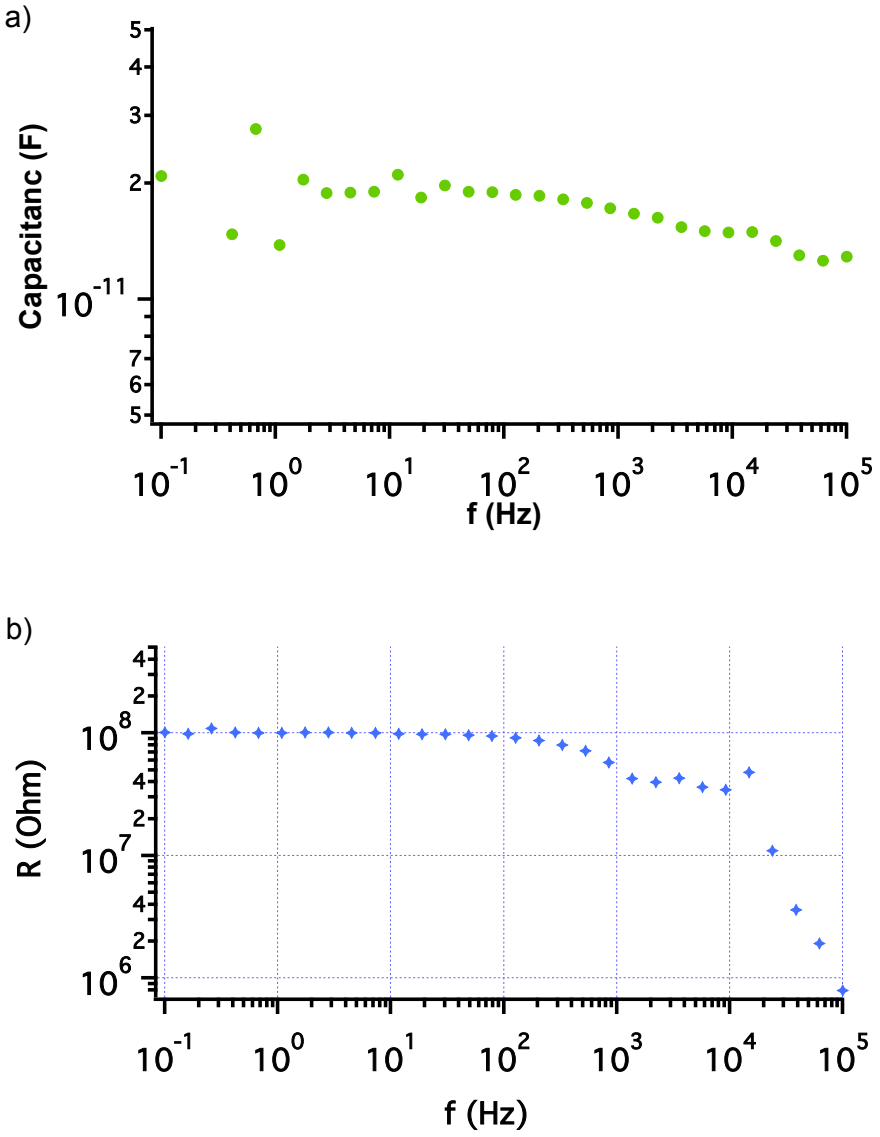

Figure 3.4: Measurements of a dummy cell consisting of parallel combination of a 100 MΩ resistor and 10 pF capacitor. a) The capacitance measurement as a function of frequency. b) The resistance measurement as function of frequency. The resistance shows noisy behaviour in the 10^3 and 10^5 Hz range.

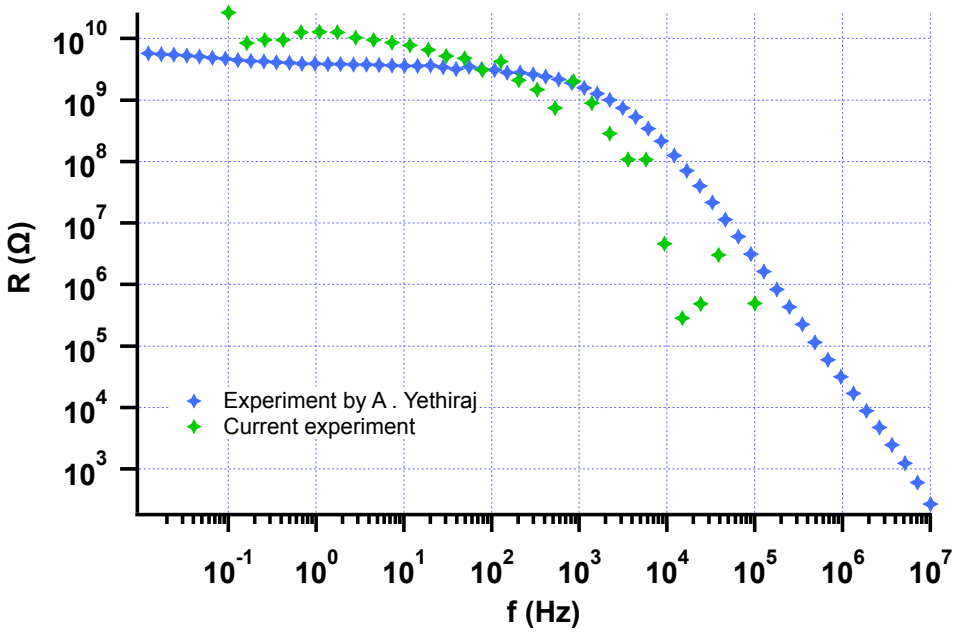

Figure 3.5: Measurements of the resistance of castor oil comparing with experiment of the same solvent but (different brand) carried out on a Novocontrol Alpha-A dielectric spectrometer, Surajit Dhara lab, University of Hyderabad.

Table 3.2: A comparison of corrections that have made to different solvents if the indicated value of stray capacitance is assumed by using the two methods, when C^{stray}= 9.3 pF and C^{stray}= 8 pF. The former was used for stray capacitance correction. The meaning of $\epsilon_{plateau}$ was explained in chapter 4.

solvents	$\epsilon_{plateau}$ when $C^{stray} = 8$	$\epsilon_{plateau}$ when $C^{stray} = 9.3$
CHB	7.53 ± 0.19	7.97 ± 0.08
Decalin	1.951 ± 0.004	2.039 ± 0.005
Decane	1.862 ± 0.005	1.982 ± 0.005
Castor oil	4.641 ± 0.039	4.71 ± 0.04

Table 3.3: Dielectric constant of CHB, Decalin, Decane, and Castor oil determined from Refs: [1, 2, 3, 4]

solvents	ϵ_{ref}	σ_{ref}
CHB	7.92	(0.1 - 0.8) μS/m
cis-Decalin	2.176	0.5 $\times 10^{-12}$ S/m
Decane	1.99	
Castor oil	4.45	(10^{-9} - 10^{-11}) S/m

3.5 Summary of practical considerations

The resistance of each sample was calculated as a function of frequency from the real part of the impedance:

$$R = \frac{1}{(\frac{1}{Z})'} \,. \tag{3.2}$$

The conductivity σ was obtained from this resistance,

$$R = \left(\frac{1}{\sigma}\right)\left(\frac{1}{G}\right) \,, \tag{3.3}$$

where G =A/d is the cell constant. The conductivity of each sample as a function of frequency could in fact be obtained either from the real part of the impedance or, equivalently, from the imaginary part of the capacitance (C'').

$$\sigma(\omega) = \left(\frac{1}{Z}\right)'\left(\frac{1}{G}\right) \,, \text{ or} \tag{3.4}$$

$$\sigma = \frac{C_{im}\omega}{G}\,. \tag{3.5}$$

The powerSUITE software reported raw data in both formats. Similarly, the dielectric constant for each sample was calculated from the imaginary part of the impedance or from the real part of the capacitance (C'),

$$\varepsilon(\omega) = \left(\frac{1}{Z}\right)'' \left(\frac{1}{\omega\varepsilon_o G}\right)\,, \text{ or} \tag{3.6}$$

$$\varepsilon(\omega) = \frac{C_{re}}{\varepsilon_o G}\,. \tag{3.7}$$

Chapter 4

Results and Discussion

4.1 Introduction

This chapter employs results from impedance spectroscopy for sample cells with three electrode spacings, in order to uncover the effects of electrode polarization. This chapter also discusses the polarization effect at low frequency for several solvent ionic strengths and cell thicknesses. The dielectric properties and the dielectric relaxation behaviour of colloidal suspension will be presented in this chapter.

4.2 Dielectric spectroscopy measurement

Dielectric spectroscopy measurements were made on several organic solvents of varying polarity: cyclohexyl bromide (CHB), cis+trans-decahydronaphtalene (decalin), castor oil and decane, as well as a mixtures of CHB-decalin. These measurements were made over a wide range of frequencies (100 mHz-100 kHz) using three sample cells of three different electrode spacing. The complex impedance Z was calculated by using Ohm's law in an alternating current (AC) circuit and converted to a frequency dependent

conductivity and dielectric constant using the relationship

$$\begin{aligned} \frac{1}{Z(\omega)} &= G[\sigma(\omega) + j\omega\varepsilon_o\varepsilon_m(\omega)] \\ \varepsilon_m(\omega) &= \left(\frac{1}{Z}\right)'' \left(\frac{1}{\omega\varepsilon_o G}\right) \\ \sigma(\omega) &= \left(\frac{1}{Z}\right)' \left(\frac{1}{G}\right) \end{aligned} \tag{4.1}$$

where the real part represents the conductivity and the imaginary part represents the dielectric constant of the measured solvent or suspension.

4.3 Dielectric properties

Figure 4.1 (a) shows the magnitude of the impedance |Z| as a function of frequency for 4 different solvents; CHB, castor oil, decalin, and decane. All solvents have some common behaviours. Log |Z| versus log f always shows linear behaviour above a threshold frequency. The slope of this power law is -1, indicating $|Z| \propto 1/f$ above a certain frequency. Bellow this frequency, |Z| exhibits a plateau. Decalin and decane exhibit only a simple power-law behaviour over the entire frequency range. Castor oil exhibits a lower |Z| ($|Z| = 11$ GΩ) but also shows a plateau at $f < 0.2$ Hz and linear behaviour at $f > 0.2$ Hz. CHB is markedly different with |Z| exhibiting a plateau for $f < 10^3$ Hz. The plateau part (or the frequency independent behaviour) at low frequencies in the impedance measurement indicates the electrolyte resistance (ohmic conduction behaviour). As the frequency decreases, the ions have time to move towards the electrodes. Thus, the ions accumulate at the electrodes and this leads to an absence of the current in the bulk of the sample; this phenomenon is known as electrode polarization. [5, 28, 29]. However, the linear behaviour at high frequencies indicates the electrolyte capacitance (non-ohmic conduction behaviour).

Acording to Equation 2.17, |Z| = R at low frequencies. Moreover, taking the log on both sides of Equation 2.17, one sees that at high frequencies

$$\log|Z| \sim \text{-}\log(f) - \log(2\pi C) \tag{4.2}$$

where the slope here is -1 indicating $|Z| \propto 1/f$ at high frequencies, and the intercept is - log(2π C).

The impedance fit function, see Equation 2.17, is a good fit to the data shown in Figure 4.1 (a), however, only part (the magnitude of |Z|) of the information can be obtained, such as the resistance R and the capacitance C of the sample. If one uses the full complex Z, one can get both ε and σ as a function of frequency.

From Figure 4.1 (b) the dielectric constant of each solvent is calculated from the imaginary part of the complex impedance Z as a function of frequency from Equation 4.1. As shown in this Figure, the dielectric constant was taken by averaging results over the frequency in the range where electrode polarization does not affect impedance. For example, the dielectric constant of CHB was taken by averaging the data between 100 Hz to 100 kHz. The dielectric constant was corrected in all our data for the stray capacitance that has been observed in chapter 3.

Figure 4.1 (c) shows the conductivity of each solvent which is calculated from the real part of the complex impedance Z from Equation 4.1. CHB has the highest ionic conductivity and thus the highest conductivity among the solvents. The conductivity of CHB is frequency independent in the range 10^{-1} to 10^{5} Hz. Castor oil has a conductivity that is 4 orders of magnitude smaller than CHB, and for other solvents, it is 2 order of magnitude lower than castor oil. The conductivity of each sample was taken at low frequencies, for example, the conductivity of castor oil was taken by averaging the data at $f < 1$ Hz. The conductivity of castor oil, decalin,

and decane increased at high frequency and the reason is not known. It should be noted, however, that the system is designed for aqueous systems, and the most polar solvents with the smallest conductivities present the biggest measurement challenge. The instrument technicians told us that 10^{-10} to 10^{-12} S/m was at the edge of the instrument sensitivity, σ could be significantly different at different frequency ranges.

The dielectric constants of the 4 solvents that are taken from the high frequency plateaux of each ε versus f plot are in good agreement with the reported values within experimental errors, as shown in Table (4.1). Furthermore, the conductivity of the 4 solvents as reported in Table (4.2) is taken from the low frequency range. The conductivity of CHB that we measured is higher than the standard result. This may be because CHB that was used in this study is unpurified and was measured as received. In addition, decalin also had different (higher) conductivity value than the standard result for cis-decalin; no literature value for the cis+trans-decalin used in this study was available. The experimentally obtained conductivity of the castor oil is consistent with the literature value.

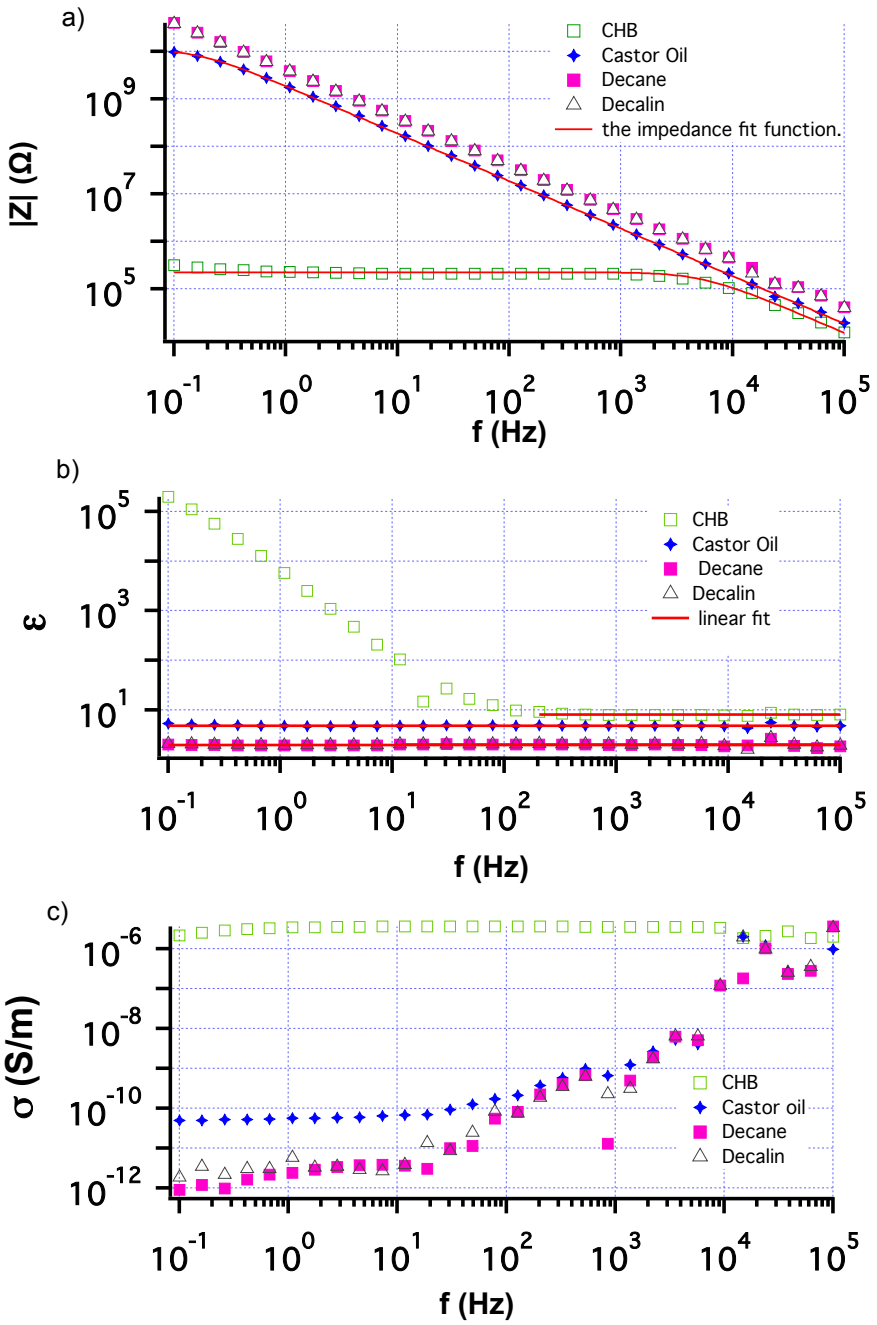

Figure 4.1: The impedance |Z|, dielectric constant ε and the conductivity σ as a function of frequency for different solvents. The impedance |Z| for decalin and decane are very close to each other. The cell constant of these measurements is G = 1.73 m.

Table 4.1: Experimental measurements of the dielectric constant of CHB, cis+trans-decalin, decane, and castor oil by using the formula $\varepsilon(\omega) = (\frac{1}{Z})''(\frac{1}{\omega\varepsilon_o G})$ and compare it with the reported values from Refs: [1, 2, 3, 4]

solvents	$\varepsilon_{plateau}$ observed from our experiments	ε_{ref}
CHB	7.97 ± 0.08	7.92
Decalin	2.039 ± 0.005 (cis+trans)	2.176 (cis)
Decane	1.982 ± 0.005	1.99
Castor oil	4.71 ± 0.04	4.45

Table 4.2: The conductivity measurements of CHB, decalin, decane, and castor oil using the formula $\sigma(\omega) = (\frac{1}{Z})'(\frac{1}{G})$ and the the absolutes values from Refs: [1, 2, 3, 4]

solvents	σ_{low} observed from our experiments	σ_{ref}
CHB	(3.2 ± 0.2) $\times 10^{-6}$ S/m	(0.1 - 0.8) 10^{-6} S/m
Decalin	(3.1 ± 0.3) $\times 10^{-12}$ S/m	0.5 $\times 10^{-12}$ S/m
Decane	(1.5 ± 0.3) $\times 10^{-12}$ S/m	
Castor oil	(5.3 ± 0.1) $\times 10^{-11}$ S/m	(10^{-9} - 10^{-11}) S/m

4.4 Electrode polarization

As discussed in section 2.9, electrode polarization (EP) is caused by the ability of ions to move and arrange as a layer along the electrodes surface at low frequencies. As a result, the applied voltage will drop across these layers leading to electrode polarization [24, 25]. EP presents a major impediment for dielectric spectra measurements of solvents or colloidal suspension properties [31].

Here we studied the electrode polarization that appears below an upper cutoff frequency f_c, which is affected by several factors, such as, the electrode separation [8, 24, 35, 36], and concentration of ions of the electrolyte or medium [8].

According to Schwan (1966), the effects of polarization impedance components (C_p , R_p) that are in a series with the sample admittance components(C_s , R_s) can be approximated by the following equations:

$$R = \left[1 + (R\omega C)^2\right] \left[R_p + \frac{R_s}{1 + (R_s\omega C_s)^2}\right] \tag{4.3}$$

$$\frac{1}{\omega C} = \left[1 + \frac{1}{(R\omega C)^2}\right] \left[\frac{1}{\omega C_p} + \frac{1/\omega C_s}{1 + (1/R_s\omega C_s)^2}\right] \tag{4.4}$$

4.4.1 Analyzing polarization impedance-Model function

Figure 4.2 shows the capacitance and the resistance of CHB as functions of frequency that we measured at small electrode distance (d = 287μm) in a log-log plot. In fact, the resultant polarization capacitance and resistance decrease as the frequency increases and this decrease behaviour can be characterized by the general power law model ($R_p = Af^{-n}$ and $C_p = Bf^{-m}$), where n and m are the power factors, while A and B

are constant values [36]. From Figure 4.2 (a), we found that the capacitance increases and dominates the signal at low frequencies. However, the solvent or suspension capacitance and resistance (C_s and R_s) can be observed only at high frequencies where the effect of electrode polarization is absent. Figure 4.2 (b) shows noisy data at high frequency above 10^4 Hz when the spectrometer change the ranges.

Figure 4.3 shows the plot of the measured ωRC of CHB as a function of frequency. We derived (see section 2.9.2) a model function from Equation 4.3 and 4.4:

$$R\omega C = \frac{\frac{1}{\omega C_p} + \frac{1/\omega C_s}{1+(1/R_s\omega C_s)^2}}{R_p + \frac{R_s}{1+(R_s\omega C_s)^2}}\,, \tag{4.5}$$

that captures the frequency dependence. This model function allows us to get the fit parameters C_p, R_p, C_s, and R_s where the last two parameters can be obtained from the high frequency plateaus of C and R. Only the polarization impedance components (C_p , R_p) need to be fitted. From the fit function, we found that C_p is not constant and it is frequency dependent with the value of $((9.71 \pm 0.7) \times 10^{-6}) f^{-0.27}$, where we defined it as $C_p = C_{p0} f^{-m}$ in the fit function as represented by power law [36]. On the other hand, the fit parameter R_p appears not to be relevant in our measurement. The calculated value from the fit function was negative, so we fixed it to be zero and it did not affect the quality of the fit adversely. The minimum that is shown in 4.3 (a) is referred to here as the electrode polarization upper cutoff frequency f_c. The intersection of the two asymptotes of the data at both low and high frequencies gives us the cutoff frequency f_c, as seen in Figure 4.3 (b). f_c represents the frequency below which ions migration to the electrodes contribute to the observed impedance. In addition, this frequency can be visualized also as the inverse of the time it takes for ions to drift from bulk solution to the electrodes.

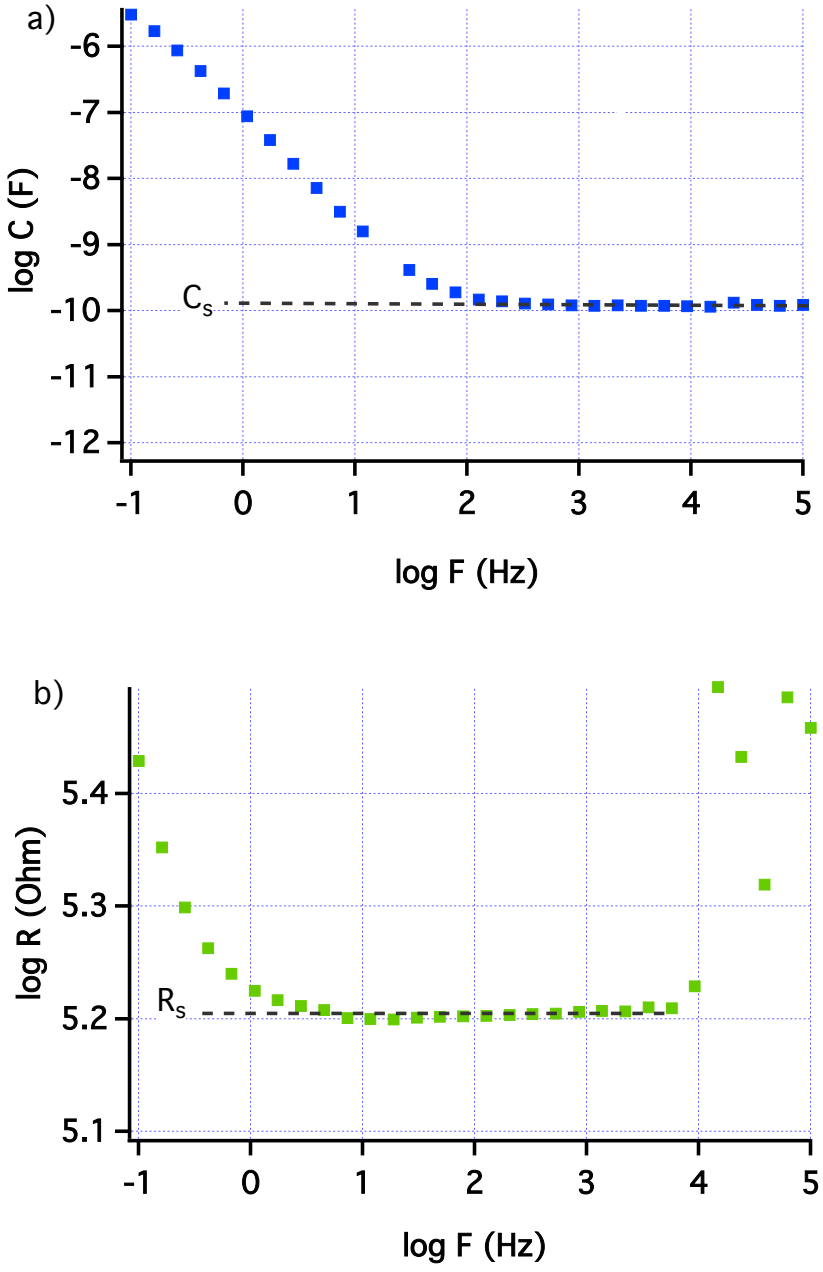

Figure 4.2: The resultant capacitance and resistance as a function of frequency of CHB solvent where the cell thickness of this measurement is (d = 276 μm). The dashed lines indicate the capacitance C_s and resistance R_s of the solvent that can been measured at high frequencies.

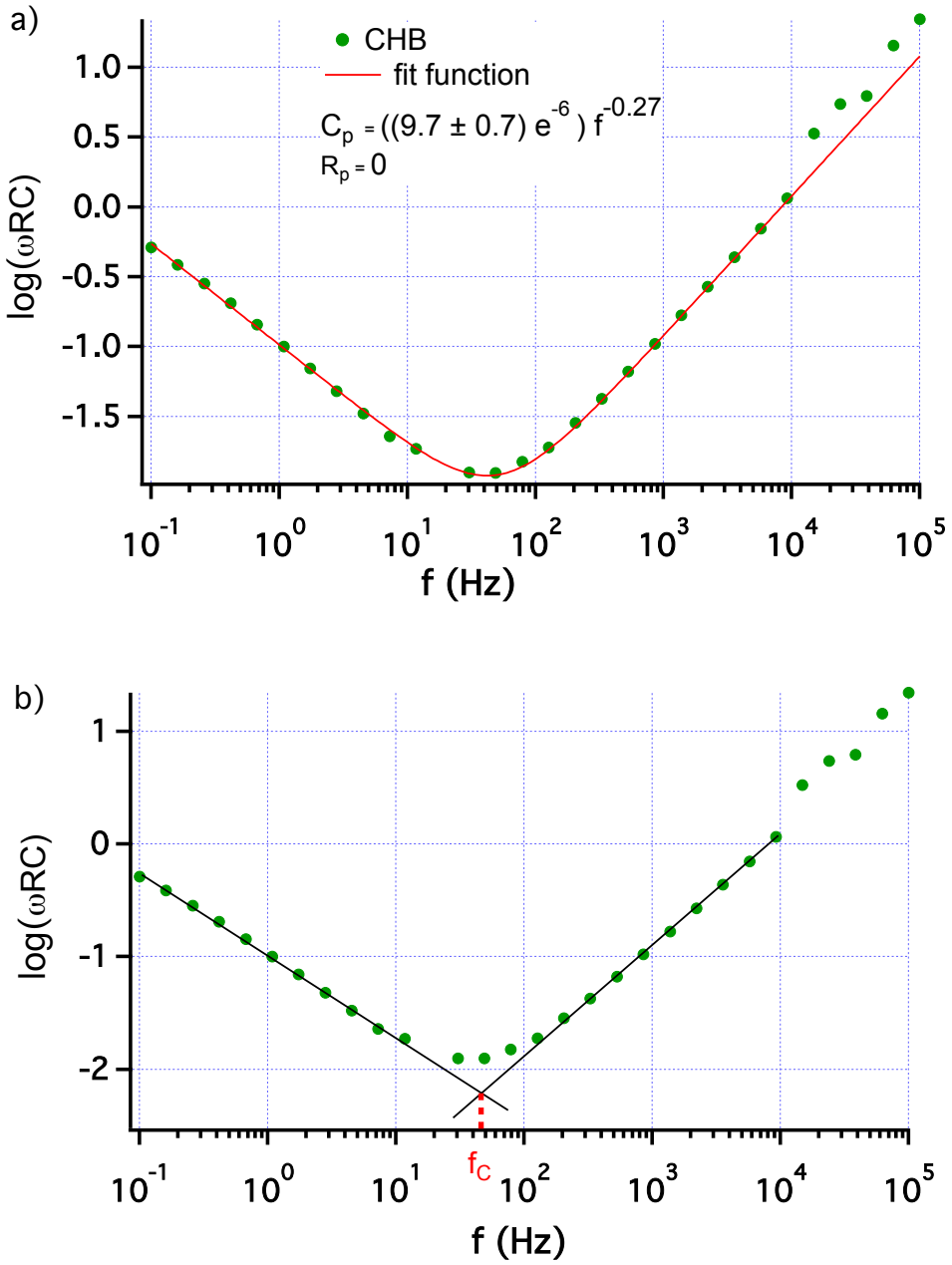

Figure 4.3: The measured ωRC as a function of frequency of CHB solvent where the cell thickness of this measurement is (d = 276 μm). a) C_p and R_p were calculated from the fit function 4.5. C_p applies power law assumption ($C_p = Bf^{-m}$) while R_p was set to zero. b) f_c is the electrode polarization upper cutoff which was measured as the point of intersection of two black linear fits at low and high frequency.

4.4.2 Electrode spacing dependence of the polarization contribution

We measured the capacitance and the resistance of CHB at three different electrode spacings d, which are 287 μm, 355 μm and 614 μm in order to study the relation between electrode polarization and the electrode spacing d. Figure 4.4 shows the measured ωRC of CHB as a function of the electrode spacing d and the frequency. When the electrode polarization upper cutoff f_c was measured at different electrode spacing, it was found that f_c decreases as d increases, as seen in Figure 4.5 (a). As d increases, $1/C_s$ in the fit function (Equation 4.5) increases, then the contribution from the polarization part in the fit function is less important. Figure 4.5 (b) shows the calculated power m from the definition of C_p ($C_p = C_{p0}\, f^{-m}$) in Equation 4.5, as function of electrode spacing d. When d increases, the power factor m decreases (but only marginally, within error bars). This behaviour means that the effect of electrode polarization is reduced as d increases. The effect of electrode polarization disappears as we find that the frequency dependence of ωRC becomes independent of d at high frequency, which reflects the behaviour of the solvent's resistance R_s and capacitance C_s.

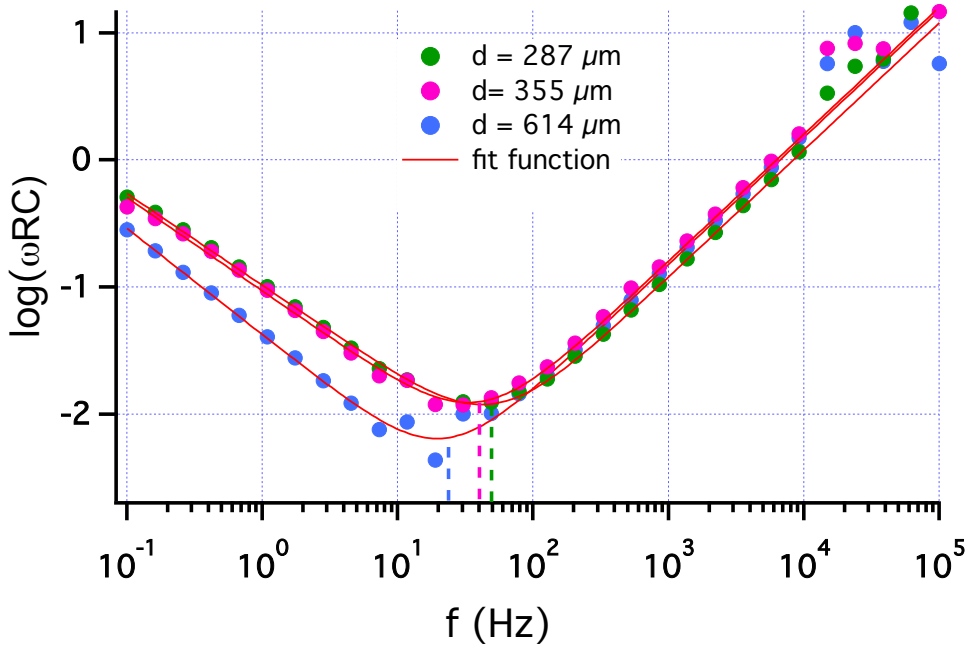

Figure 4.4: The measured ωRC as a function of frequency of CHB for three different electrode spacings d. The dashed lines represent the cutoff frequency f_c.

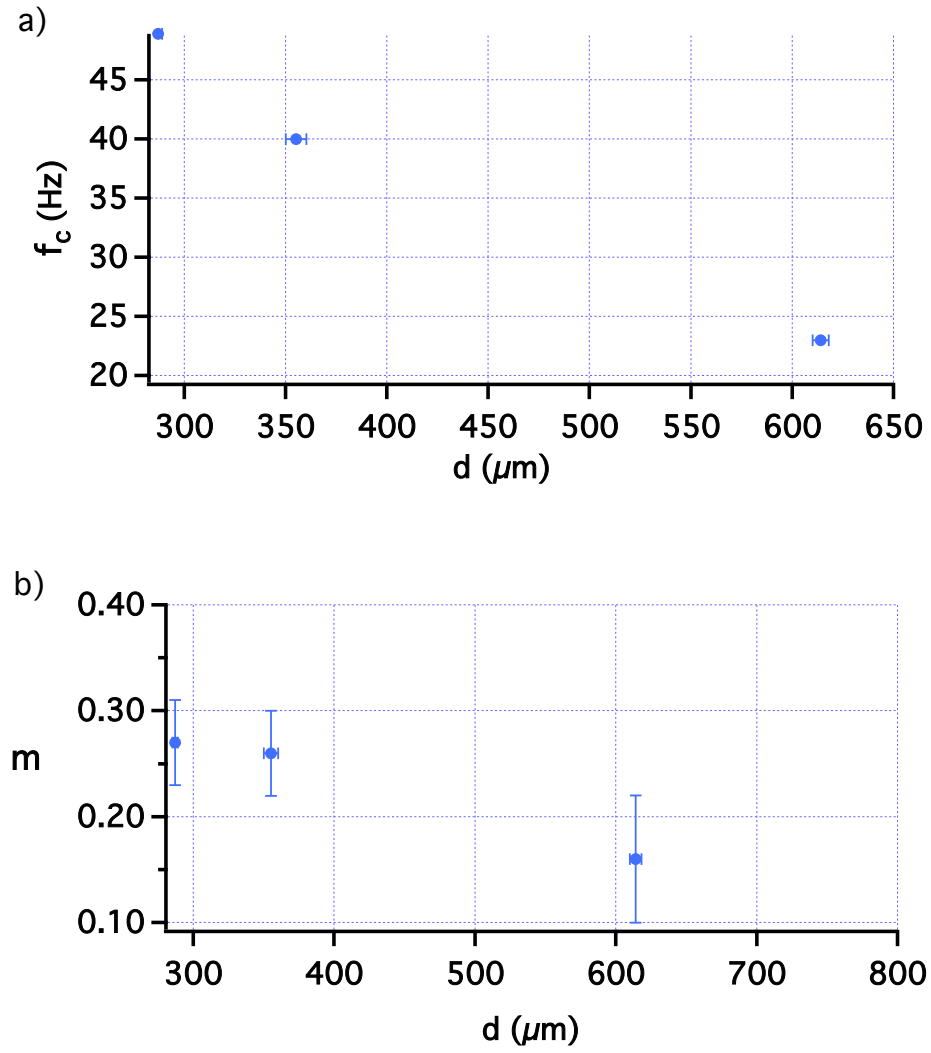

Figure 4.5: a) The electrode polarization upper cutoff f_c as a function of the electrode spacing d. b) The calculated power factor m from the definition of C_p ($C_p = C_{p0}\, f^{-m}$) in Equation 4.5, as function of d.

4.4.3 Electrode polarization for different solvent conductivities

The electrode polarization is most important for CHB, which has the highest ionic conductivity among the solvents. As one decreases ion concentration, we would expect to reduce the electrode polarization effect. We test this by examining mixtures of CHB with two solvents of lower conductivity, dodecane and decalin. In Figures 4.6 we plot $\varepsilon_{plateau}$ (taken from the plateau part of ε as a function of ω (the weight fraction of dodecagon and decalin in CHB)). In Figure 4.7 (a), we plot σ (taken from the low frequency range) as a function of w. Figure 4.7 (b) shows $\ln(\sigma)$ vs ω. The log plot indicates that $\ln(\sigma)$ has a linear relation with the weight fraction, which indicating an exponential dependence on w. From this fit, we can obtain a dependence $\sigma = \sigma_0 \exp^{(-w/w_0)}$ where σ_0 is the CHB conductivity and $w_0 = \frac{1}{14.3} = 0.07$.

We found that as the weight fraction of decalin and dodecane increases the dielectric constant and conductivity decrease. Next in Figure 4.8, we carry out the same electrode polarization analysis as for pure CHB.

Figure 4.8 (a) and (b) shows the measured ωRC of mixtures of CHB with dodecane and decalin solvents respectively. As the weight fraction of decalin and dodecane increases, f_c decreases as seen in Figure 4.9 (a). As w increases as ε decreases and thus the fitted $1/C_s$ in Equation 4.5 increases. Thus the contribution from the polarization part becomes smaller. Figure 4.9 (b) shows the power factor m with large error bars, thus it is hard to distinguish if m increases or decreases with d within theses large error bars. So we took the average of all points and we got a constant m of ($m \approx 0.25 \pm 0.04$).

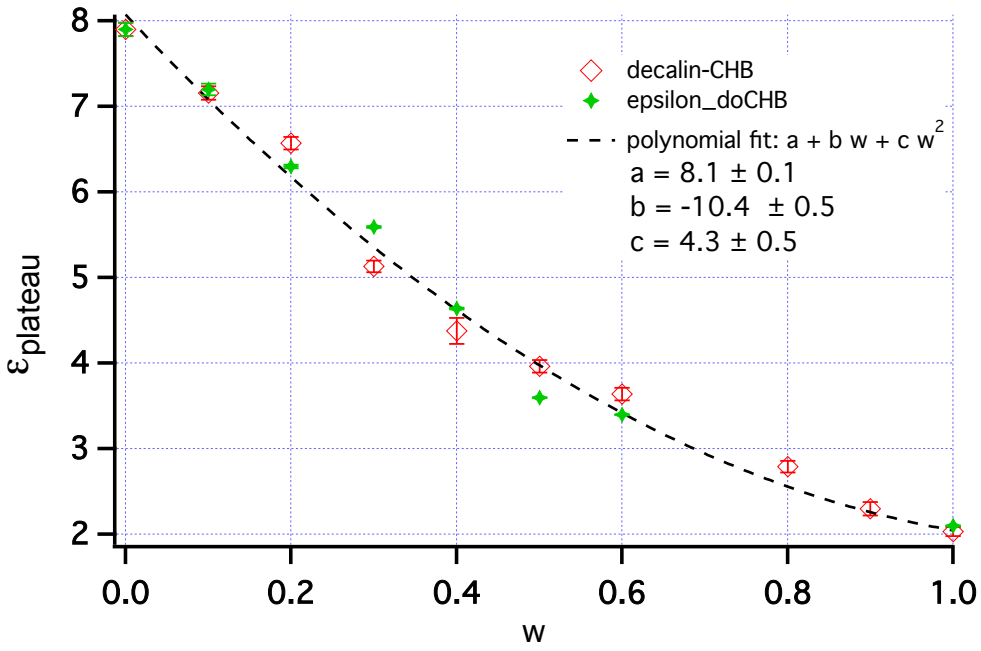

Figure 4.6: The dielectric constant of two mixtures, decalin-CHB and dodecane-CHB as a function of weight fraction of dodecane or decalin in CHB, where the dashed line is the polynomial fit. The cell thickness in theses measurements is 276 μm.

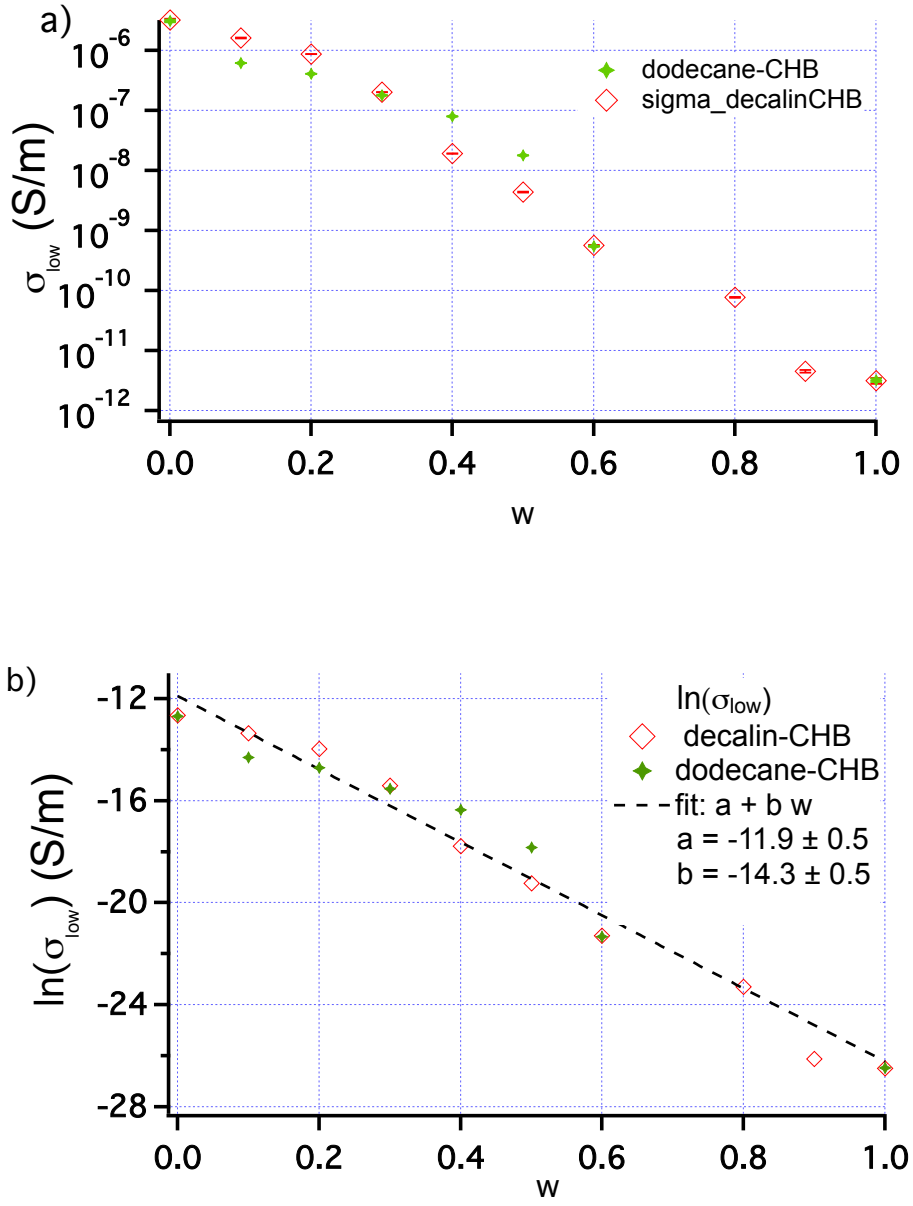

Figure 4.7: a) The conductivity of two mixtures, decalin-CHB and dodecane-CHB as a function of weight fraction of dodecane or decalin in CHB. b) Log of the conductivity of the two mixtures where the dashed line is the linear fit. The cell thickness in theses measurements is 276 μm.

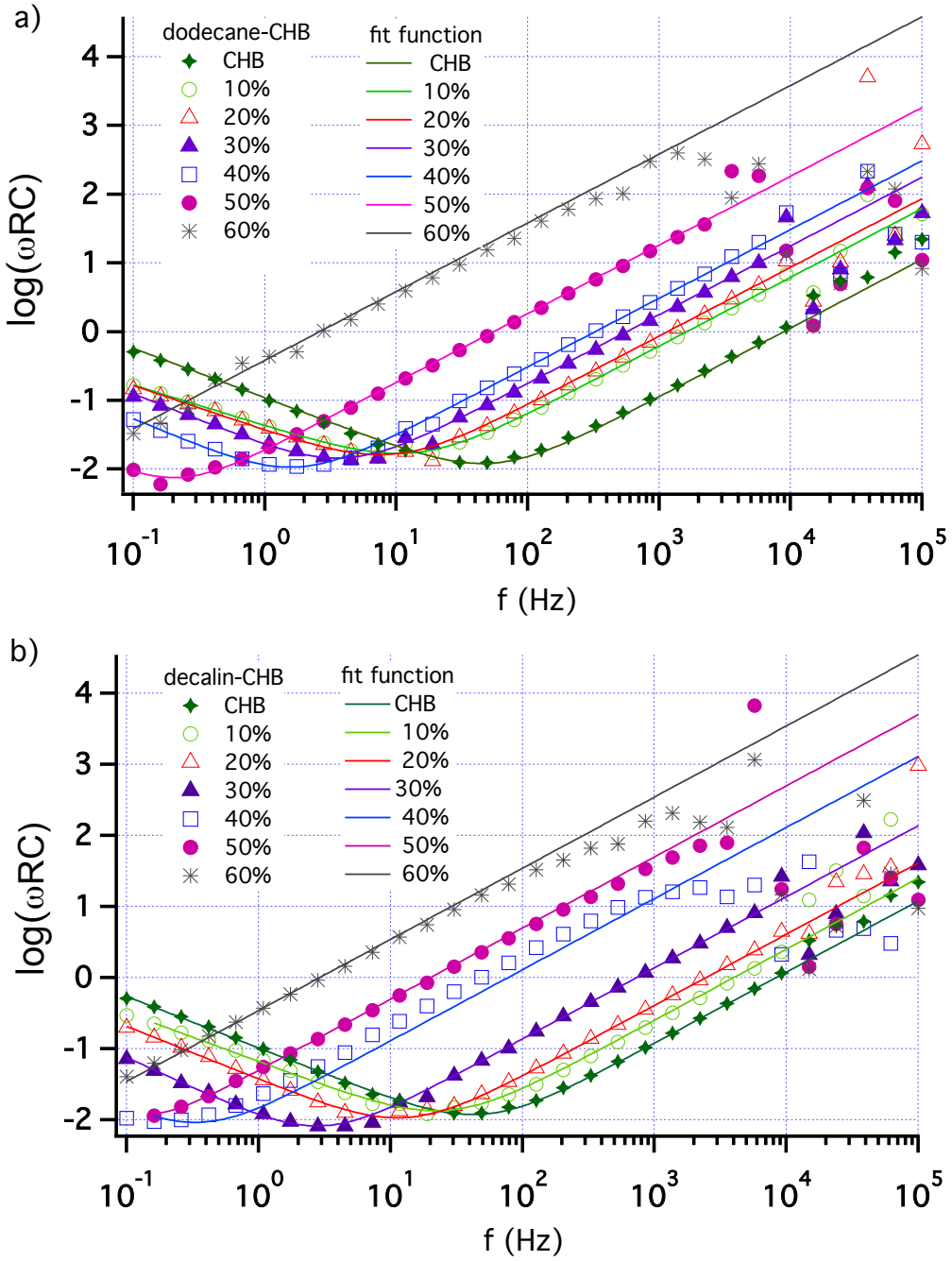

Figure 4.8: a)The measured ωRC of dodecane-CHB mixture as a function of weight fraction of dodecane in CHB and frequency. b) The measured ωRC of decalin-CHB mixture as a function of weight fraction of decalin in CHB and frequency. The cell thickness in theses measurements is 276 μm.

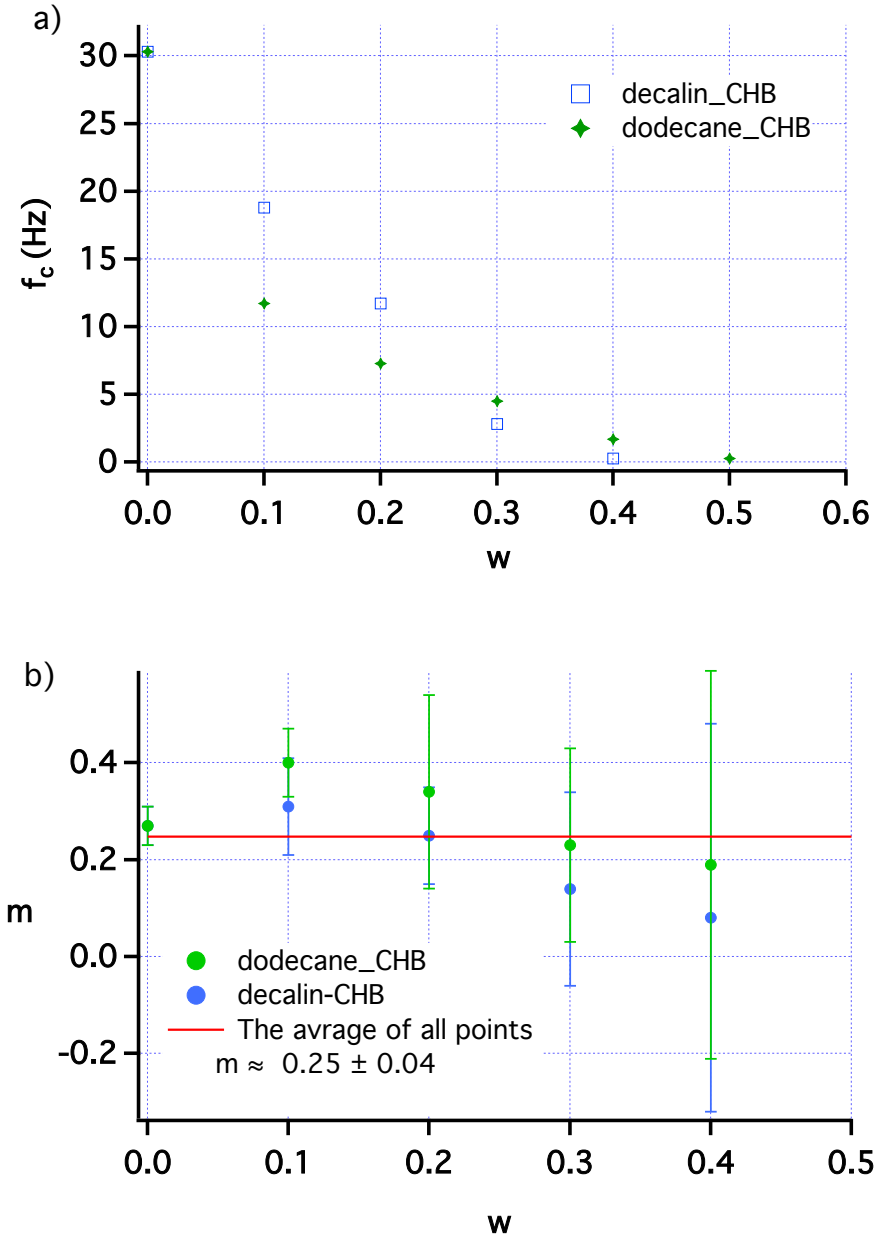

Figure 4.9: a) The electrode polarization upper cutoff f_c obtained from the fits in Figure 4.8 as a function of wight fraction w. b) The calculated power factor m from the definition of C_p ($C_p = C_{p0}\, f^{-m}$) in the fit function Equation 4.5, as function of weight fraction w that also obtained from the fits in Figure 4.8. The red line is the average of all 10 points.

Figure 4.10 shows the plots of the power m and f_c for CHB measurement of 3 different thickness that we have obtained in Figure 4.4, and for the mixture of 20% decalin-80% CHB, as a function of d. This is a useful test for electrode polarization. Figure 4.10 (a) shows the power $m \approx 0.26 \pm 0.01$ when d increases, where m was taken by averaging the all 6 points. From figure 4.10 (b) we found that as we increase the electrode spacings and decrease the ionic concentration in the electrolyte (mixture of 20% decalin-80% CHB), the electrode polarization upper cutoff f_c decreases. We fitted the data to 1/d and we found that a specific minimum electrode spacing range can be recommended for experiments at any given frequency.

For example, let us consider an electric field experiment on a colloidal suspension to be carried out at $f = 10$ Hz. We extend the fit function to large d where f_c crosses 10 Hz this is at ($d \sim 2$mm). This is the minimum cell thickness that should be used, if there is interest in studying the low-frequency characteristics of a colloidal suspension, in order to avoid the electrode polarization effect. Therefore, one can identify from these plots that, for example, for a study at 10 Hz, the electrode separation should be > 1.5 mm.

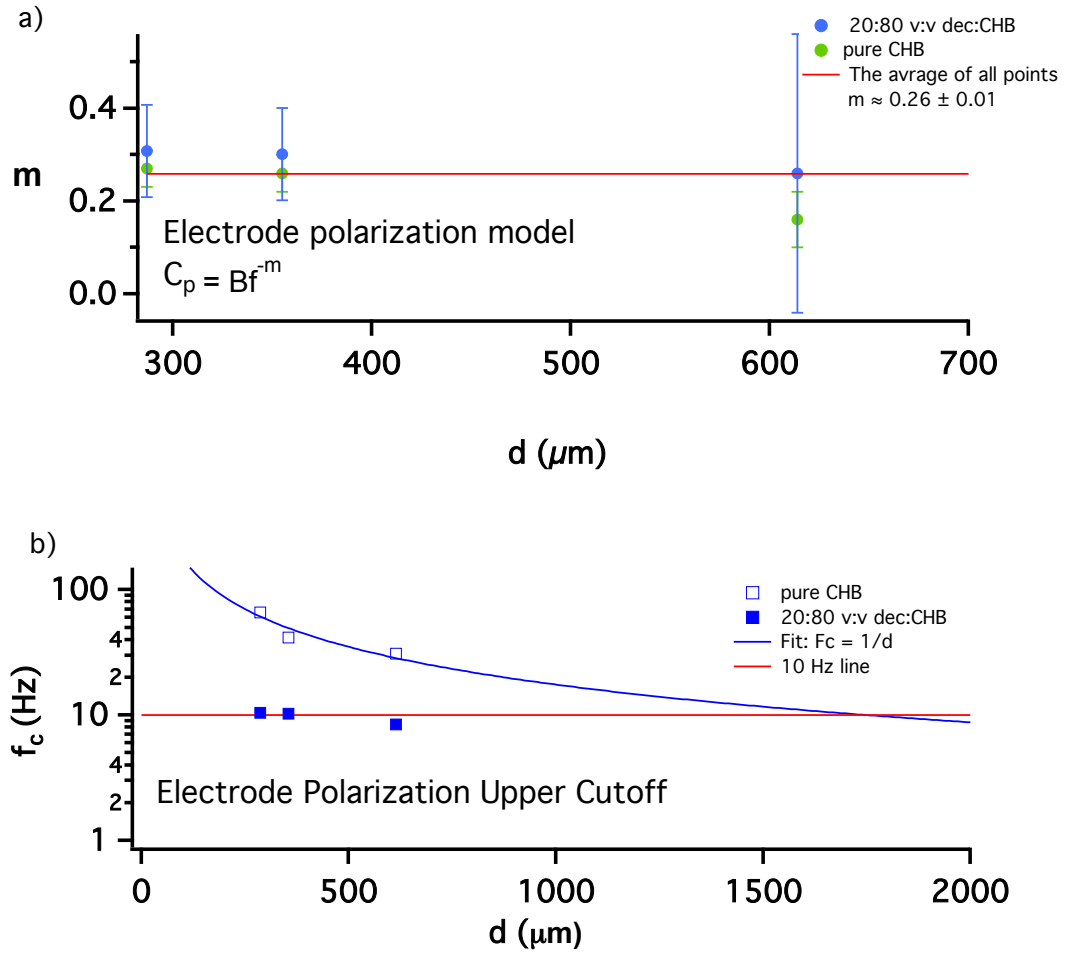

Figure 4.10: a) The power factor m for the polarization capacitance ($C_p = Bf^{-m}$) of CHB and CHB-decalin mixture (20:80 v:v) as a function of d. b) The electrode polarization upper cutoff f_c of CHB and CHB-decalin mixture as function of d. The data was extrapolated to cross $f_c = 10$ Hz, see section 4.6.2.

4.5 Debye length κ^{-1}

Figure 4.11 shows the dielectric constant ε, the ions concentration C_i, and the Debye screening length $\kappa^{-1}$of decalin-CHB mixtures measurement as a function of increasing decalin by weight. Figure 4.11 (a) shows that the dielectric constant ε of CHB-decalin mixture is decreasing with increasing the weight fraction of decalin because we add low polar solvent of dielectric constant smaller than CHB. The conductivity is proportional to the ion concentration, so when the ion concentration C_i of the medium decreases the conductivity decreases. This decreasing behaviour was observed when we increased the amount of cis+trans-decalin in the mixture, which is indicating that the ion dissociation is decreasing as well, as shown in Figure 4.11 (b). Debye length κ^{-1} depends on ε and the degree of the dissociation of ions. The latter depends on the ion concentration and the dielectric constant of the medium. As a result, as the weight fraction increases, and consequently the ion concentration decreases, the Debye screening length growth exponentially from 0.1 μm to 54 μm as seen in Figure 4.11 (c).

We calculated Debye screening lengths, κ^{-1}, by applying Walden's rule to the conductivity data [17]. This rule states that the product of the limiting equivalent molar conductance Λ and the viscosity η are constant between different media, i.e $\Lambda^m\eta^m = \Lambda^w\eta^w$, where m here refers to the mixture and w refers to water. Thus, we calculated first Λ^m for each concentration by using Walden's rule $\Lambda^m = \frac{\Lambda^w\eta^w}{\eta_m}$, where Λ^w and η^w for water is 146 S.cm^2/mol and 0.894 mPa.s respectively [38]. From Λ^m, we calculated C_i by using the following relation

$$C_i\,[mol/L] = \sigma\,[S/m] \times \frac{1}{10^3\Lambda^m}\,[mol/S.m^2] \tag{4.6}$$

Then Debye screening lengths, κ^{-1}, can be determined

$$\kappa^{-1} = (0.344 \times 10^{-10}\, m)\sqrt{\frac{\epsilon}{C_i}} \tag{4.7}$$

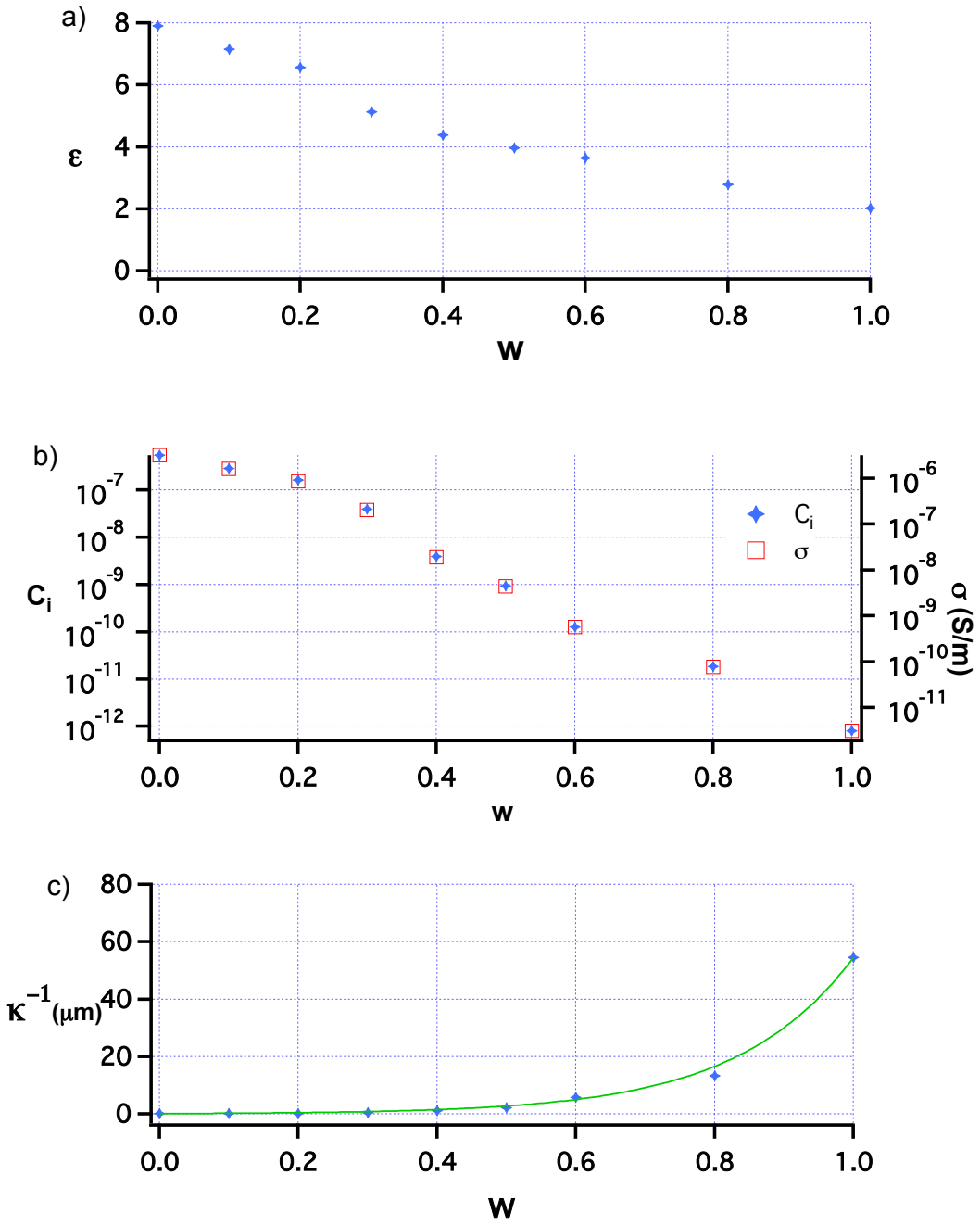

Figure 4.11: The dielectric constant ε, the ions concentration C_i, and the Debye screening length $\kappa^{-1}$of decalin-CHB mixture measurement as a function of increasing decalin by wight. Debye screening lengths, κ^{-1}, was estimated by applying Walden's rule to conductivity data.

4.6 Colloids

4.6.1 Dielectric properties of the suspension

A small part of this work is about the dielectric spectroscopy response of colloidal suspension. This was originally the primary goal, but understanding issues surrounding electrode polarization in particle-free solvents became a large focus. We suspended several volume fraction of PMMA particles (ASM447) ($\phi = 0.05$ and 0.1) of radius 1μm and dielectric constant of 2.6 [39] in cyclohexyl bromide (CHB) with 20% cis+trans-decahydronaphthalene by volume. The dielectric constant of this solution, as shown in 4.12 (b), is 6.6.

Figure 4.12 (a) shows the dielectric constant as a function of frequency for solvent and for two volume fractions of PMMA particles. The dielectric constant of the suspensions was taken from the frequency independent part of the spectrum, between 100 Hz and 10 kHz, where below 100 Hz we see the electrode polarization effect and above 10 kHz the data was found to be noisy as seen in Figure 4.12 (b). Furthermore, we found that the dielectric constant of the suspension decreased as the particle volume fraction increased, see Figure 4.12 (b), this is because the high dielectric constant CHB-decalin mixture solvent ($\varepsilon = 6.6$) is replaced by low dielectric constant particles ($\varepsilon = 2.6$ [39]). The measured values were compared with the calculated values, as seen in Figure 4.12 (c). The caculated value was obtained from the following equation

$$\varepsilon_{calc} = \phi\varepsilon_p + (1 - \phi)\varepsilon_m \tag{4.8}$$

Since this calculated dielectric constant would be exact if the particles and solvent were parallel plate capacitors in parallel, we expected this to be an upper bound. The calculated value is, however, lower than the measured value and we don't have clear explanation for this behaviour, therefore, more studies are needed in this suspension.

Figure 4.13 (a) shows the conductivity of the same suspensions that are shown in Figure 4.12 as a function of frequency. From the conductivity measurements of the colloidal suspensions that are shown in Figure 4.13 (a), we found that the conductivity is frequency independent below 10 kHz and above this frequency the data is noisy. In addition, the conductivity decreased when the particle volume fraction increased which means that the particles did not significantly releases ions into solution. If we replace the electrolyte by uncharged particles, we will get a more non-conducting suspension, thus the conductivity will decrease [21]. The measured values were compared with the calculated values, as seen in Figure 4.13 (b). The calculated value was obtained again as indicative estimate, equivalent to resistors in parallel,

$$\sigma_{calc} = \phi\sigma_p + (1 - \phi)\sigma_m \tag{4.9}$$

Once again, this should be an upper bound, provided that no ions are released. Here we set σ_p =0, and we found that the measured value is lower than the calculated value. There is a physically meaningful possibility. If particles were stuck on the electrode surface, this would correspond to resistors in series, and the conductivity would be smaller (the particles would effectively block the current).

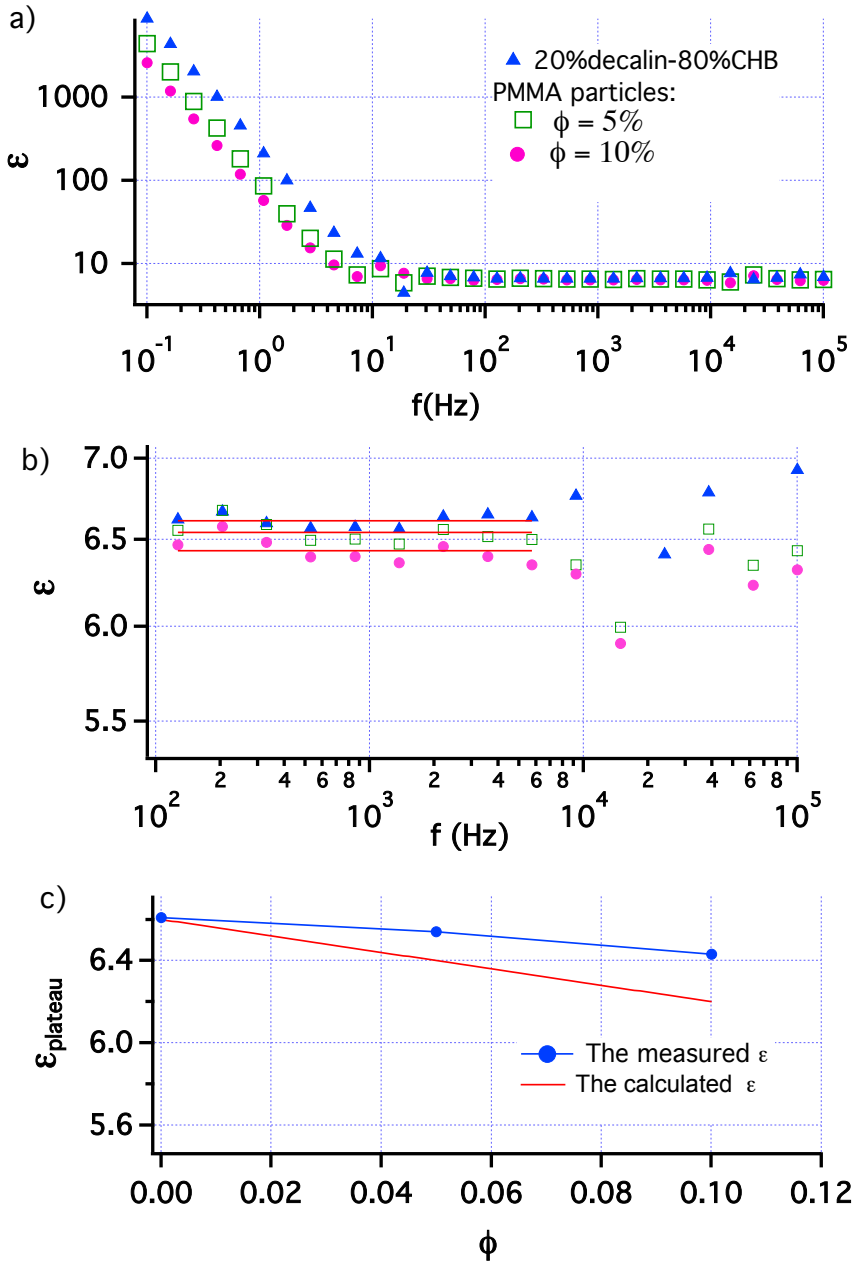

Figure 4.12: a) The dielectric constant of the suspensions as a function of particle volume fraction and frequency. b) It is a magnification of panel a) at high frequency range between 10 kHz to 10 kHz, the red lines correspond to the averaging ε. c) The dielectric constant as a function of volume fraction of of the suspensions shown in panel (a) and it was compared with the calculated value from equation 4.8.

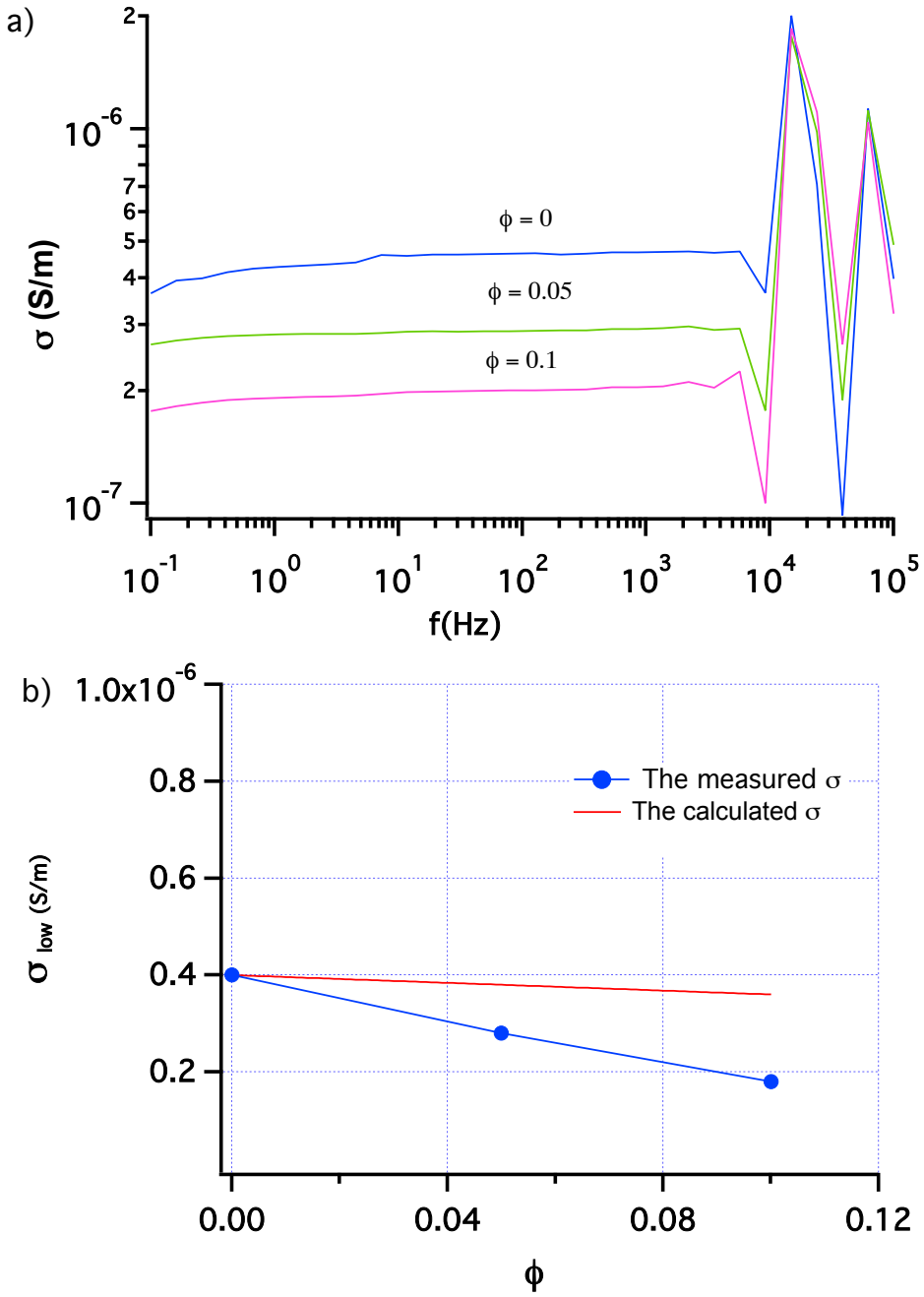

Figure 4.13: a) The conductivity of the suspensions as a function of particle volume fraction and frequency. b) The conductivity as a function of volume fraction of the suspensions shown in panel (a), and it was compared with the calculated value from Equation 4.9.

4.6.2 Dielectric relaxation

PMMA particles exhibit dielectric relaxation due to migration of charged species in solution. Figure 4.12 (a) shows the dielectric constant ε as function of frequency and particle volume fraction. Once again, $\varepsilon \propto 1/f$ at low frequencies, below 10 Hz, and a frequency independent ε is seen above 10 Hz. While the dielectric relaxation is expected to result in step-like changes as the frequency increases, this behaviour didn't show up in our measurement, see Figure 4.12 (a).

The characteristic frequency of the double layer relaxation f_{rel} can be calculated from the simple dimensional analysis, assuming an effective particle radius of $a + \kappa^{-1}$:

$$f_{rel} = \frac{\omega}{2\pi} \approx \left(\frac{D_{ion}\kappa^2}{2\pi(1+\kappa a)^2} \right) . \tag{4.10}$$

This estimated characteristic relaxation frequency f_{rel} in our suspension measurement was calculated with $D_{ion} \approx 0.5 \times 10^{-5}\ cm^2/\text{s}$, $a = 1\ \mu\text{m}$, and $\kappa^{-1} = 0.3\ \mu\text{m}$. Here, D_{ion} is the diffusion coefficient of the counter-ions that are surrounded the charged particle, a is the particle radius, and κ^{-1} is the Debye length. In our non-aqueous system, we found that the characteristic frequency is about 35 Hz. It is possible that the magnitude of this relaxation is small, and thus not seen because it falls within the region where the effect of electrode polarization is observed. Thus, the plateau of the dielectric constant at very low frequencies, or the step-like behaviour as the frequency increases was not observed in our measurement. Correction of this electrode polarization error is need to study the dielectric relaxation process.

In an aqueous system that was studied by Saville (1990), the characteristic frequency of the double layer relaxation is different [12]. We calculated it by using the same Equation 4.10 and we found that when one increased the ionic strength in the solution by adding 1mM of HCl , the Debye length decreased to about 8 $\times 10^{-9}$m. In

this study, the particle radius was 113nm and $D_{ion} \approx 0.5 \times 10^{-5}\ cm^2/\text{s}$. As a result, the characteristic frequency increased, it was about 6kHz which is higher than that observed in non-aqueous system due to a smaller (a + κ^{-1}).

To conclude these results, the characteristic relaxation frequency f_{rel} increases by increasing the concentration of ions or decreasing the particle radius, as seen in Table (4.3). In fact, the smaller particles radius, the smaller dipole moment induced by the external field. The smaller particles means the shorter path that ions need to follow around particles, and the shorter time is needed to induce that dipole moment and hence a shorter relaxation time or larger relaxation frequency [40]. In order to observe colloidal relaxation, the cell must be thicker than 1.5mm (according to Figure 4.10 (b)), in order to avoid artifacts from electrode polarization to hide suspension characteristics.

Table 4.3: The calculated characteristic relaxation frequency f_{rel} and Debye length κ^{-1} with decreasing particle radius a in aqueous and non-aqueous systems.

System	a μm	κ^{-1} μm	f_{rel}
non-aqueous	1	0.3	35 Hz
aqueous	0.113	0.008	6 kHz

4.7 Discussion

The dielectric properties of cyclohexyl bromide (CHB), cis+trans-decahydronaphtalene (decalin), castor oil, decane, and mixtures of CHB-decalin that have been observed in this study are in good agreement with the standard results within experimental error, as shown in Table (4.1) and (4.2). The conductivity measurement of CHB is higher than the standard result. This is possibly because CHB that was used in this study is unpurified and was measured as received. Ohmic and non ohmic conduction, which are the resistance and the capacitance parts, respectively, are observed on CHB and castor oil solvents in the impedance plot as we expected from the following equation (the impedance fit function):

$$|Z| = \frac{R}{\sqrt{1 + (2\pi RfC)^2}} \tag{4.11}$$

This equation indicates that at low frequency the capacitance part may be ignored, thus the resistance part will dominate, while at high frequency the capacitance part is large and will dominate. However, a simple power-law behaviour is observed on decalin and decane solvents (capacitance part) because these solvents have low polarity and hence high resistance.

Electrode polarization has been found in CHB measurement at low frequencies in the range of (0.1Hz - 50 Hz). We derived the fit function, Equation 4.5, that describes the behaviour of the curve in Figure 4.3 and the electrode polarization components can be calculated. The fit function calculated only the polarization capacitance C_p, where it was defined in the fit function as $C_p = C_{p0}\, f^{-m}$ from the power law [36]. We found that C_p for CHB is frequency dependent with the value of $((9.71 \pm 0.7) \times 10^{-6}) f^{-0.27}$ (F): it tells us that the polarization capacitance at f =1 Hz is 9.7 μF. In addition, we

have shown how the electrode polarization upper cutoff f_c depends on the electrode spacing and the concentration of ions. As we increase d and/or decrease the concentration of ions, as the mobility of ions decreases which leading to decreasing the electrode polarization. Comparing with results that have been observed by Schwan (1966) for platinum electrodes and more higher conductive sample (sample of blood), we have found comparable polarization behaviour, ($i.e., R_p$ and C_p decrease as the frequency increases). Schwan found that the power factor m is 0.4, where (m) increases as the frequency increases from 0.3 to 0.5 between 0.01 kHz to 100kHz [24]. In this study, we found the effect of electrode polarization was observed only in the solvent capacitance C_p, while R_p was indistinguishable from Zero, and m was about 0.25 ± 0.04. On the other hand, Schwan observed the effect of electrode polarization in both capacitance and resistance. This different result was possibly because of the large difference in conductivity in aqueous solvents in comparison with the partially polar CHB. From both measurements, the effect of electrode polarization on C and R decreases as C_p increases [8]. In addition, it is clear that the model for electrode polarization proposed by Schwan [36] is well satisfied in our measurements.

The dielectric properties of colloidal suspension was studied in this work. We found that the dielectric constant was decreasing with increasing particle volume fraction. In fact, when a solvent that contains a high dielectric constant of 6.6 is replaced by particles with low dielectric constant of 2.6, the resultant suspension will has lower dielectric constant [11]. On the other hand, we found that the conductivity of the suspension decreased when the particle volume fraction increased which means the particles did not significantly release ions into solution. A study by Vissers (2011) [22] also showed that the conductivity of the suspension decreases as the particle volume fraction increases and this behaviour referred to the effect of adding insulating

PMMA particles in the solvent. The double layer relaxation was calculated for our non-aqueous system and compared with an aqueous system that has been observed by Saville (1990) [12]. We found that the characteristic relaxation frequency f_{rel} increases by increasing the concentration of ions or decreasing the particle radius. The smaller particles means the shorter path that ions need to follow around particles, and the shorter time is needed to induce that dipole moment and hence a shorter relaxation time or larger relaxation frequency [41].

Chapter 5

Conclusions

Dielectric properties as a function of frequency of some low-polar solvents, cyclohexyl bromide (CHB), cis+trans-decahydronaphtalene (decalin), castor oil and decane, as well as a mixtures of CHB-decalin have been measured in this study. The dielectric constants of the 4 solvents are in good agreement with the standard results within experimental errors. However, the conductivity of CHB was found to be higher than the result abstained previously with distilled CHB. No standard value was available for cis+trans-decalin.

Electrode polarization (EP) that appears at an upper cutoff frequency f_c is an important issue that has been found at low frequencies in CHB measurement, between (0.1Hz - 50 Hz). The electrode polarization can be reduced by increasing the electrode spacing and/or decreasing the concentration of ions (mixture of CHB-decalin or CHB-dodecane). A fit function was modelled, Equation 4.5, to describe the physical phenomena of the dielectric spectra at low and high frequencies. The polarization parameter C_p have been obtained from the fit function. The capacitance C_p was frequency dependant $C_p = C_{p0}\, f^{-m}$ i-e a power law that decreases when the frequency increases. We found that the power $m \approx 0.25 \pm 0.04$ for a range of electrode spacings

and ionic concentrations. We also found the electrode polarization upper cutoff f_c depends on the electrode spacing and the concentration of ions.

The Debye screening length κ^{-1} has been estimated for CHB-decalin mixtures as a function of increasing decalin by weight. We found that the Debye screening length grows roughly exponentially from 0.1 μm to 54 μm as we increased the amount of decalin, or as the ion concentration was decreased.

In colloidal suspension, the dielectric constant was decreasing with increasing colloidal particle volume fraction because the dielectric constant of the particle is smaller than that in the medium. In addition, the conductivity of the suspension decreased when the particle volume fraction increased. Two challenging issues were recorded from the dielectric constant of the colloidal suspension measurements, electrode polarization effect at low frequencies, below 100 Hz, and noisy data at high frequency above 10 kHz. Thus, the dielectric relaxation, which is of great interest to understand colloid electrokinetics, was not seen in our system. We calculated the predicted characteristic relaxation frequency f_{rel} for our non-aqueous system and aqueous system by Saville (1990) [12]. We found that f_{rel} increases by increasing the concentration of ions or decreasing the particle radius. In our non-aqueous system, we found that the characteristic frequency f_{rel} is between 10 and 35 Hz.

For future work, more information can be obtained at low frequencies if the polarization contribution is corrected. In specific, in order to study the colloidal relaxation behaviour in intermediate polar media, the cell must be designed in which the polarization contribution is avoided. We suggested that the cell should be thicker than 1.5mm (according to Figure 4.10 (b)) for studying at 10 Hz, in order to avoid artifacts from electrode polarization to hide suspension characteristics. The characteristic frequency of the colloid relaxation can also be increased a bit by reducing particle size. For example, based on Equation 4.10, reducing particle size to 0.2 μm would result in

$a + \kappa^{-1} \approx 0.5$ μm, increasing the relaxation frequency almost seven-fold to 240 Hz. This would be ideal for future studies.

Bibliography

[1] Heston Jr W. M., Hennelly E. J., and Smyth C. P. Dielectric constants, viscosities, densities, refractive indices and dipole moment calculations for some organic halides. *Journal of the American Chemical Society*, 72:2071–2075, 1950.

[2] Staudhammer P. and Seyer W. F. The dielectric constant of cis- and trans-decahydronaphtalene and cyclohexane as a function of temperature and frequency. *Journal of the American Chemical Society*, 80, 1958.

[3] *Handbook of chemistry and physics*. The Chemical Rubber Co, 46th edition, 1965-1966.

[4] Xu X. *Electrohydrodynamic flow and chaotic mixing inside drops*. PhD thesis, University of California, 2007.

[5] Ishai P. B., Talary M. S., Caduff A., Levy E., and Feldman Y. Electrode polarization in dielectric measurements: a review. *Measurement Science and Technology*, 24:1–21, 2013.

[6] Barsoukov E. and Macdonald J. R. *Impedance Spectroscopy*. John Wiley and Sons, Inc, 2005.

[7] Schönhals A. and Kremer F. *Broadband Dielectric Spectroscopy*. Springer-Verlag Berlin Heidelberg GmbH, 2003.

[8] Schwan H. P. Linear and nonlinear electrode polarization and biological material. *Annals of Biomedical Engineering*, 20:279–288, 1992.

[9] Beltramo P. J., Roa R., Carrique F., and Furst E. M. Dielectric spectroscopy of concentrated colloidal suspensions. *Journal of Colloid and Interface Science*, 408:54–58, 2013.

[10] Delgado A. V., González-Caballero F., Hunter R. J., Koopal L. K., and Lyklema J. Measurement and interpretation of electrokinetic phenomena. *Journal of Colloid and Interface Science*, 309:194–224, 2007.

[11] Leunissen M. *Manipulating Colloids with Charges Electric Fields*. PhD thesis, Utrecht University, 2007.

[12] Rosen L. A. and Saville D. A. Dielectric spectroscopy of colloidal dispersions: comparisons between experiment and theory. *Langmuir*, 7:36–42, 1990.

[13] Mittal M., Lele P. P., Kaler E. W., and E. M. Furst. Polarization and interactions of colloidal particles in ac electric fields. *The Journal of Chemical Physics*, 129:064513, 2008.

[14] Beltramo P. J. and Furst E. M. Predicting the disorder–order transition of dielectrophoretic colloidal assembly with dielectric spectroscopy. *Electrophoresis*, 34:1000–1007, 2013.

[15] Tao R. and Jiang Q. Simulation of structure formation in an electrorheological fluid. *Physical Review Letters*, 73:205–208, 1994.

[16] Yethiraj A. Tunable colloids: control of colloidal phase transitions with tunable interactions. *Soft Matter*, 3:1099–1115, 2007.

[17] Yethiraj A. and van Blaaderen A. A colloidal model system with an interaction tunable from hard sphere to soft and dipolar. *Nature*, 421(513-517), 2003.

[18] Leunissen M. E., van Blaaderen A., Hollingsworth A. D., Sullivan M. T., and Chaikin P. M. Electrostatics at the oil-water interface, stability, and order in emulsions and colloids. *Proceedings of the National Academy of Sciences*, 104:2585–2590, 2007.

[19] Beltramo P. J. and Furst E. M. Transition from dilute to concentrated electrokinetic behavior in the dielectric spectra of a colloidal suspension. *Langmuir*, 28:10703–10712, 2012.

[20] Hayden E. Colloidal dynamics in the presence of oscillatory electrophoretic forces, 2013.

[21] Russel W. B., Saville D. A., and Schowalter W. R. *Colloidal Dispersions: theory, experiment, and applications*. The Press Syndicate of the University of Cambridge, 1989.

[22] Vissers T., Imhof A., Carrique F., Delgado A. V., and Van Blaaderen A. Electrophoresis of concentrated colloidal dispersions in low-polar solvents. *Journal of Colloid and Interface Science*, 361:443–455, 2011.

[23] Swan J. W. and Furst E. M. A simpler expression for henry's function describing the electrophoretic mobility of spherical colloids. *Journal of Colloid and Interface Science*, 388:92–94, 2012.

[24] Schwan H. P. Electrode polarization impedance and measurement in biological materials. *Annals of the New York Academy of Sciences*, 148:191–209, 1968.

[25] Bockris J. O. and Reddy. *Modern Electrochemistry an Introduction to an Interdisciplinary Area*. Berlin: Springer, 1973.

[26] Bonanos N., Pissis P., and Macdonald J. R. Impedance spectroscopy of dielectrics and electronic conductors. *Characterization of Materials*, 2012.

[27] Pohl H. A. *Dielectrophoresis: The behaviour of Neutral Matter in Nonuniform Electric Fields*. Cambridge University Press, 1978.

[28] McAdams E. T., Lackermeier A., McLaughlin J. A., Macken D., and Jossinet J. The linear and non-linear electrical properties of the electrode-electrolyte interface. *Biosensors and Bioelectronics*, 10:67–74, 1995.

[29] Sanabria H. and Miller Jr J. H. Relaxation processes due to the electrode-electrolyte interface in ionic solutions. *Physical Review E*, 74:051505, 2006.

[30] Lyklema J. *Fundamental of interface and colloid science*. Academic Press Inc, 1995.

[31] Myers D. F. and Saville D. A. Dielectric spectroscopy of colloidal suspensions: I. the dielectric spectrometer. *Journal of Colloid and Interface Science*, 131:448–460, 1989.

[32] Helmholtz H. On the some laws of the distribution of electrical current in material conductors with application to experiments in animal electricity. *Poggend. Annals*, 89:269–278, 1853.

[33] Warburg E. Ueber das verhalten sogenannter unpolarisirbarer elektroden gegen wechselstrom. *Annalen der Physik*, 303:493, 1899.

[34] Fricke H. The theory of electrode polarization. *The London, Edinburgh, and Dublin Philosophical Magazine and Journal of Science*, 14:310–318, 1932.

[35] Schwan H. P. *Physical Techniques in Biological Research*. Academic Press Inc, 1963.

[36] Schwan H. P. Alternating current electrode polarization. *Biophysik*, 3:181–201, 1966.

[37] Cirkel P. A., Van der Ploeg J. P. M., and Koper G. J. M. Electrode effects in dielectric spectroscopy of colloidal dispersions. *Physica A: Statistical Mechanics and its Applications*, 235:269–278, 1997.

[38] Bockris J. O. M. and Reddy A. K. *Modern electrochemistry, Volume 1: Ionics*. Journal of Chemical Education, 1999.

[39] Mikhailov G. P. and Borisova T. I. The dielectric investigation of molecular relaxation in polymers. *Russian Chemical Reviews*, 30:386–396, 1961.

[40] Carrique F., Arroyo F. J., and A. V. Delgado. Effect of size polydispersity on the dielectric relaxation of colloidal suspensions: A numerical study in the frequency and time domains. *Journal of Colloid and Interface Science*, 206:569–576, 1998.

[41] Carrique F., Jiménez M. L. Arroyo F. J., and Delgado A. V. Dielectric response of concentrated colloidal suspensions. *The Journal of Chemical Physics*, 118:1945–1956, 2003.